

MINERALOGICAL STUDY OF DAVIS MINE, ROWE, MASSACHUSETTS, USING X-RAY DIFFRACTION TECHNIQUES

Department of Geosciences
University of Massachusetts, Amherst
Amherst, MA 01003

An Independent Study Presented

by

Amy B. Cerato

Submitted September 2003

ABSTRACT

Davis Mine was a sulfide mine operated from 1890 to 1911. The overflowing groundwater drains out of the old mine shafts with an acidity lower than vinegar (pH around 2) and carries large loads of heavy metals. The mine has been producing acidic runoff for the past eight decades and may attenuate this acid mine drainage through Fe (III) sulfate reduction and the presence of microorganisms. The physical characteristics of the acid mine drainage (AMD) site of importance are the mineralogy, particle size, physical weathering tendencies and permeability. The particle size (mineralogy) relates to the amount of surface area that is exposed to oxidation.

This report provides a general description of the mineralogy of the Davis Mine site using X-Ray Diffraction (XRD) techniques. This report also documents the grain-size of the soils and estimates hydraulic conductivity of the soil overlying the bedrock using predictive methods. Thirty samples were collected from throughout the site to map the mineralogy and hydraulic conductivity. From this study, it has been found that most of the samples contain the original rock-forming clay minerals chlorite and mica with many samples containing the potassium iron sulfate hydroxide, jarosite. Jarosite is a product of sulfide oxidation, which is abundant throughout the site and is found in varying quantities depending on the depth of the sample. Each XRD test was performed using the glass slide method and tested with Cu-K alpha radiation.

The average hydraulic conductivity of the site was calculated using four grain-size predictive methods, which ranged from 1.5 to 3.0×10^{-4} m/s (42 to 83 ft/day). These values correlate well with previous bail tests performed on site and are representative of a fine sand aquifer (Freeze and Cherry 1979).

Table of Contents

Abstract	i
Table of Contents	ii
List of Tables and Figures.....	iii
1.0 Introduction	1
2.0 Background	1
2.1 History of Davis Mine	1
2.2 Brief Background into Acid Mine Drainage.....	3
2.3 Hydrological Setting	6
2.4 Mineralogy	7
2.4.1 Mineralogy of Davis Mine.....	7
2.4.2 Mineralogy of Tailings	8
2.5 X-Ray Diffraction	10
2.6 Hydraulic Conductivity.....	11
2.6.1 Grain-Size Predictive Methods	11
2.6.2 Previous Work – Mine Tailings.....	16
3.0 Experimental Program	18
3.1 Grain-Size Analysis	20
3.2 XRD Sample Preparation.....	21
3.2.1 Slide Treatments	22
3.2.3 Diffractogram Generation	23
4.0 Results	24
4.1 Grain-Size Analysis	24
4.2 XRD Analysis	27
4.2.1 Air-Dried Oriented Glass Slide.....	29
4.2.2 Glycolated Oriented Glass Slide.....	50
5.0 Discussion	55
5.1 Hydraulic Conductivity.....	55
5.2 Mineralogy	56
6.0 Summary and Conclusions	61
7.0 References	62
Appendix A Grain-Size Analysis Figures and Data Sheets.....	65
Appendix B Full Size AirDried Diffractograms.....	98
Appendix C Full Size Glycolated Diffractograms.....	134

LIST OF TABLES

Table 2.1	Hazen (1911) Coefficients for Determining Hydraulic Conductivity	14
Table 2.2	Values for Uma et al. (1989) Empirical Coefficient.....	14
Table 2.3	Hydraulic Conductivity Results of the Tailings Pile (after Gal 2000).....	18
Table 3.1	Soil Sample Log and Soil Descriptions	20
Table 4.1	Grain-Size Distribution Results	25
Table 4.2	Hydraulic Conductivity Predictive Method Results	26
Table 4.3	Average Hydraulic Conductivity Values in Well Profiles.....	27
Table 4.4	Mineral Contents in the Clay Fraction of the Samples by XRD Analysis.	28
Table 4.5	Common d-Spacings in Å for Typical Clay Minerals	28
Table 4.6	Common d-Spacings in A for Typical Non-Clay Components	29
Table 5.1	Comparison of Average Hydraulic Conductivity Predictive Method Results.....	55

LIST OF FIGURES

Figure 2.1	Location of Davis Mine in Massachusetts	2
Figure 2.2	Site Plan of Davis Mine	7
Figure 2.3	Hydraulic Conductivity Relationship to Mean Grain Size (from Shepard 1989)	15
Figure 3.1	Location Map of Soil Samples.....	21
Figure 4.1	Diffractiongram for Well 6 – 1’	30
Figure 4.2	Diffractiongram for Well 7 – 1’	30
Figure 4.3	Diffractiongram for Well 7 – 2’	31
Figure 4.4	Diffractiongram for Well 7 – 3’	32
Figure 4.5	Diffractiongram for Well 7 – 3.25’	33
Figure 4.6	Diffractiongram for Well 7 – 3.5’	33
Figure 4.7	Diffractiongram for Well 7 – 4’	34
Figure 4.8	Diffractiongram for Well 7 – 5’	35
Figure 4.9	Diffractiongram for Well A – 1’	36
Figure 4.10	Diffractiongram for Well A – 2’	36
Figure 4.11	Diffractiongram for Sample 02-01.....	37
Figure 4.12	Diffractiongram for Sample 02-03.....	37
Figure 4.13	Diffractiongram for Sample 02-07.....	38
Figure 4.14	Diffractiongram for Sample 02-09.....	39
Figure 4.15	Diffractiongram for Sample 02-10.....	40
Figure 4.16	Diffractiongram for Hole B – 1’	41
Figure 4.17	Diffractiongram for Hole C – 1’	41
Figure 4.18	Diffractiongram for Hole C – 2’	42
Figure 4.19	Diffractiongram for Hole C – 2.5’	42
Figure 4.20	Diffractiongram for Hole C – 3’	43
Figure 4.21	Diffractiongram for Hole C – 4’	44
Figure 4.22	Diffractiongram for Hole C – 5’	44

Figure 4.23	Diffractogram for Hole D – 1’	45
Figure 4.24	Diffractogram for Hole D – 2’	46
Figure 4.25	Diffractogram for Well 9 – 1’	46
Figure 4.26	Diffractogram for Well 9 – 2’	47
Figure 4.27	Diffractogram for Well 9 – 3’	47
Figure 4.28	Diffractogram for Well 9 – 4’	48
Figure 4.29	Diffractogram for Well 5 – 2’	49
Figure 4.30	Diffractogram for Well 2 – 2’	50
Figure 4.31	Determination of Swelling Clays in Well 6 – 1’ by the Ethylene Glycol Method	51
Figure 4.32	Determination of Swelling Clays in Well 7 – 5’ by the Ethylene Glycol Method	51
Figure 4.33	Determination of Swelling Clays in Well 9 – 3’ by the Ethylene Glycol Method	52
Figure 4.34	Determination of Swelling Clays in Well 9 – 4’ by the Ethylene Glycol Method	53
Figure 4.35	Determination of Swelling Clays in Well 5 – 2’ by the Ethylene Glycol Method	53
Figure 4.36	Determination of Swelling Clays in Well 2 – 2’ by the Ethylene Glycol Method	54
Figure 5.1	Diffractogram Results Compiled by Depth in Well 7	56
Figure 5.2	Diffractogram Results Compiled by Depth in Hole C	58
Figure 5.3	Diffractogram Results Compiled by Depth in Hole D	59
Figure 5.4	Diffractogram Results Compiled by Depth in Hole A	60
Figure 5.5	Diffractogram Results Compiled by Depth in Well 9	61

1.0 INTRODUCTION

In the recent past, acid mine drainage has become a major environmental concern due to its hazards on groundwater. The minerals of the soil ultimately control the geochemistry of the groundwater. The host rock composition, and therefore the weathered soils overlying this bedrock, together with the hydrology, climate and time since deposition are factors in the alteration, dissolution and precipitation processes within the glacial till. The Davis Pyrite Mine has remained undisturbed for over eight decades during which time the highly acidic drainage has been slowly cleaning itself. Therefore, there is a need to study the mineralogy of this site to see what role it plays in the system approaching equilibrium over an extended period of time. This report provides a general description of the mineralogy of the Davis Mine site using X-Ray Diffraction (XRD) techniques and provides an estimate of hydraulic conductivity of the soil overlying the bedrock using grain-size predictive methods. Each XRD test was performed using the glass slide method (Moore and Reynolds 1996) and tested with Cu-K alpha radiation.

2.0 BACKGROUND

2.1 History of Davis Mine

As early as 1840 it had been known that deposits of ore were in the southeastern part of Rowe (Figure 2.1).

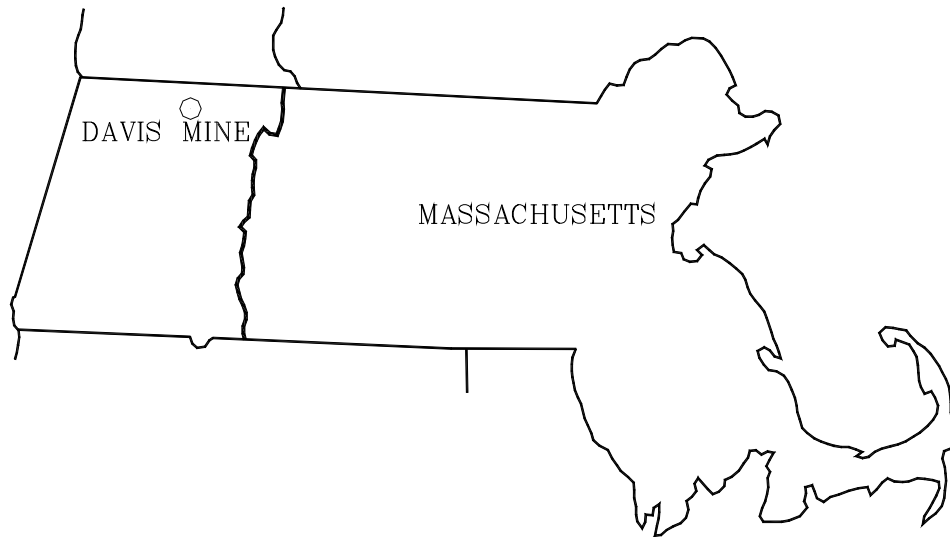


Figure 2.1: Location of Davis Mine in Massachusetts.

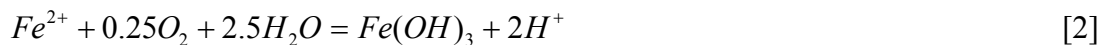
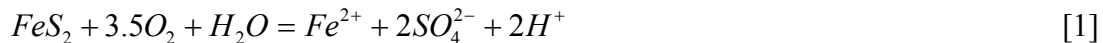
The ore was quite brassy in appearance, very similar to “Fools Gold,” and was thought to be of little value. Although few people interested in rock collecting had visited the area, no commercial value was placed on these ores until about 1880, when pyrites had begun to be used instead of brimstone in the manufacture of sulphuric acid. This fact was the catalyst behind Mr. Herbert Jerome Davis pursuing these ores as a possible new source of supply.

Mr. Davis bought the land around this ore vein and had samples analyzed. The analysis showed: Sulphur 50.15%, Arsenic 2.5%, Iron 44.15%, Zinc 3.55%, Copper 1.55% and Loss 0.35% (Brown 1960). Being comparatively free of arsenic, the ore was a major source of sulphur and was in great demand for use in the chemical industry here and overseas. The Davis Mine was said to be the most successful mine in Massachusetts and one of the finest of its kind in the country.

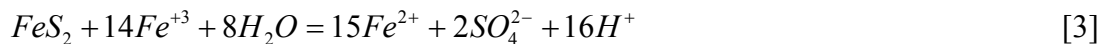
By January 1883, Davis was sending 20 tons of ore a day to Charlemont and shipping it to Boston. During 1883 a new shaft was begun and by September 1883, shipping had been increased to 500 tons per week. The mine prospered until 1909, but in time, poor mining practices caused the ore supports or pillars to weaken and some cave-ins occurred. The timber supports were not replaced as they rotted and water became more and more a problem. At last, miners began to take only the ore that was easy to reach. On a Sunday night in July 1909, everything above the fourteenth level in Shaft Number 1 caved in. After this, smaller cave-ins occurred from time to time and the operation of the mine became less profitable. For about a year, the mine existed, with difficulty, but in August 1911, this once fine operation closed (Brown 1960).

2.2 Brief Background into Acid Mine Drainage

The waters draining from many mines in the eastern United States are strongly acidic as a consequence of oxidation of pyrite and sulfide materials. The stoichiometry of the oxidation can be represented by the equations



The overall mechanism by which pyrite is oxidized in natural acidic systems can be represented better by a two-step process in which pyrite is oxidized by ferric iron:



and ferric iron is generated by microbial oxidation of ferrous iron:



The rate-determining step in this sequence is commonly the microbial oxidation of Fe^{2+} to form Fe^{3+} (Singer and Stumm 1970). At Davis Mine, these bacteria are called *Thiobacillus ferrooxidans*. Ferric iron that is not consumed in this catalytic cycle is ultimately precipitated as $\text{Fe}(\text{OH})_3$, which is the ochre/orange precipitate found in the Davis Mine Creek bed.

When streams become contaminated by acid mine drainage, adjacent vegetation dies and precipitation of ferric hydroxide occurs over long distances. The AMD process is started by oxygenated water penetrating the overburden, acquiring a certain alkalinity. The amount of this alkalinity is determined by the P_{CO_2} of the water. As the water moves through the sulfide seam picking up iron, manganese and aluminum in solution, oxidation of pyrite occurs. This generates acidity, which at first is neutralized by the alkalinity in the groundwater. If the acidity generated is greater than the initial alkalinity in the water, all the alkalinity will be consumed and acid water will result. The precipitate on the streambed occurring from the reaction of water and acid ($\text{Fe}^{3+} \rightarrow \text{Fe}(\text{OH})_3$) has a characteristic orange-red, yellow (sometimes white) color, commonly known as “yellow boy.”

The metals stay in solution beneath the earth due to the lack of oxygen. When water emerges from the mine or borehole it reacts with the oxygen in the air or dissolved in the stream and deposits iron, manganese and aluminum on rocks and the streambed. If sufficient oxygen is present, the amount of acidity generated is determined by the amount of reactive pyrite in the sulfide seam. Low pH and high dissolved metals of acid mine drainage (AMD) is toxic to fish and aquatic insects in moderate concentrations. At high concentrations all plant life is killed. In the absence of mining, acid waters are uncommon

because the large volume of permeable, fine grained sulfide generated from the mining processes are not available for groundwater to react with.

Primary, secondary, tertiary, and downstream factors influence the quality and quantity of mine drainage.

- **Primary factors** influencing the amount and quality of acidic water are the relative amount of water and oxygen in the environment. In order for pyrite to oxidize, both oxygen and water must be present. Water serves not only as a reactant, but also as a reaction medium and a product-transport solvent (Forstner, Salomons 1988).
- A **secondary factor** is the neutralization of acids by the alkalinity released from the carbonate minerals in the mine waste and surrounding stratum (Forstner, Salomons 1988).
- **Tertiary factors** include the physical characteristics of mining waste, the spatial relationship between wastes, and the hydrologic regime.

The physical characteristics of importance are particle size, physical weathering tendency, and permeability. The particle size relates to the amount of surface area that is exposed to oxidation. The smaller the particle size, the more total surface area is exposed, and the greater potential for oxidation. Weathering increases the surface area of the material. The increase in surface area and the physical weathering and fracturing of strata increase the permeability of the waste material.

The sequence of stacking different wastes may affect the water quality of mine drainage. By contributing to the alkalinity of the percolating water, calcareous material placed atop pyritic material will reduce both the potential for oxidation and the acidity

generated (Forstner, Salomons 1988). At Davis Mine, there are no calcareous materials to help neutralize the acidity.

The hydrologic regime of a mine can influence the quality of mine drainage. Because waste inundation limits the transfer of oxygen, significant acid generation in a saturated zone may not occur. A fluctuating water table induces pyrite oxidation during declines in the water table (Forstner, Salomons 1988).

Downstream factors may impact the quality and quantity of acid drainage. Physical processes such as dilution and precipitation and chemical processes such as neutralization will permit a stream to assimilate acid drainage, but not without incurring a great deal of acid damage to the preceding stream area (Forstner, Salomons 1988). This is the case at Davis mine. At the start of Davis Mine Creek, the pH is around 2. There are no life forms or vegetation throughout the Davis Mine Creek. The pH in Davis Mine Brook increase slightly after the confluence of Davis Mine Creek, and slowly increases further downstream.

2.3 Hydrological setting

Davis Mine Brook is the main stream of the area, however there is a small tributary, the “Mine Effluent Creek,” running through the study area (Figure 2.2). It is 160 m long and originates from the entrance of the mine Shaft 1. “Mine Effluent Creek” flows through the spoil pile from north to south and enters Davis Mine Brook. The Davis Mine Brook watershed is 375 m long and 200 m wide, with an average gradient of 0.11 (Gal 2000). It is covered with mixed deciduous and coniferous forest. The mean annual

precipitation is 1100 mm, and the monthly distribution of precipitation is fairly uniform throughout the year.

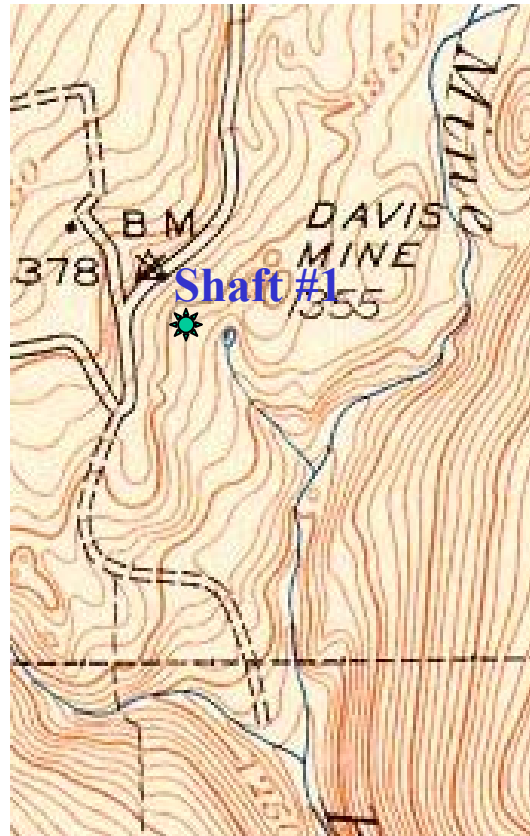


Figure 2.2: Site Plan of Davis Mine.

2.4 Mineralogy

2.4.1 Mineralogy of Davis Mine

The geologic characterization of this mine is a Fe-(Zn-Cu-Pb) sulfide ore deposit formed by hydrothermal sulfide activity in the lower part of the Hawley Formation, which formed in the middle Ordovician at about 450 Ma. Pyrite is the most abundant sulfide present, comprising 60 to 70 volume percent of the ore. A weak Cu-Zn zonation, which is a common feature of many volcanogenic massive sulfides, is present in the

deposit. The principal mineralogy of the Hawley Formation was described by Field (1985) as:

- Silicates: quartz [SiO₂], plagioclase (albite) [NaAlSi₃O₈], chlorite [(Mg,Al)₃[Si₄O₁₀(OH)₂ (Mg,Fe)₃(OH)₆], biotite [K(Mg,Fe)₃[AlSi₃O₁₀(OH)₂]], muscovite [KAl₂[AlSi₃O₁₀(OH)₂]], garnet [Mg₃Al₂[Si₃O₁₂]], hornblende [Na(Ca,Fe)₅(SiAl)₈O₂₂(OH)₂], and epidote [Ca₂(Al,Fe)Al₂[O OH SiO₄ Si₂O₇]];
- Oxides: magnetite [Fe₃O₄], gahnite [AlZn₂O₄], ilmenite [FeTiO₃], rutile [TiO₂];
- Carbonates and phosphates: ankerite [CaFe(CO₃)₂] and apatite [Ca₅[F(PO₄)₃]];
- Sulfides: pyrite [FeS₂], pyrrhotite [FeS₂], sphalerite [ZnS], chalcopyrite [Cu,FeS], and galena [PbS].

Tailings piles were distributed over an area of approximately 3 ha (7.4 acres) downstream from the mineshafts. The stream that drains the tailings piles, Davis Mine Creek, runs over a bed coated with yellow, ochre and red pigments, suggesting a complex community of microbes flourishing in the acidic environment. Except for the immediate vicinity of the mine, which is largely devoid of plant life, the area around the site is forested with a mixed hardwood community typically developed on glacial till in the upland areas in New England. The glacial till has a thickness of .5 to 5 m, as found during the drilling process. Soils in the area are generally Inceptisols (ochrepts) or Spodosols (orthods). These soils usually have organic horizons ~5-10 cm thick, with a layer of decomposing organic matter above the "A" horizon.

2.4.2 Mineralogy of Tailings

Previous work has been done regarding characterizing the mineralogy of one of the tailing piles at Davis Mine. The mine tailings pile was deposited down slope, south of the mineshafts. Gal's (2000) study was performed to determine the acid neutralization processes taking place in the tailing pile that Davis Mine Creek runs through. It is 160 m long and 30 m wide. The upper 30 m of the creek disappears during dry periods. The

tailing piles have little to no undergrowth or grass-cover and retain only a few small coniferous trees. The O soil horizon is missing and there is no distinguishable A-horizon. A hardpan layer has formed on the surface, where the slope gradient is small (1-2%) and water table is high. As there is no record of the mining and ore-separating techniques it has been presumed that the spoil was dry deposited.

Typical colors of mine tailings are from canary yellow through ochre to rusty brown. The characteristic yellow is caused by different ferric and ferrous oxyhydroxide minerals, among which some occur only in tailings. These minerals are the result of the oxidative weathering of iron sulfide minerals and they are important in the transport and attenuation of iron and trace elements in surface waters. Goethite [α -FeOOH], jarosite [$\text{KFe}_3(\text{OH})_6(\text{SO}_4)_2$], hydrobasaluminite [$\text{Al}_4(\text{SO}_4)(\text{OH})_{10} \cdot 12\text{-}36\text{H}_2\text{O}$], lepidocrocite [γ -FeOOH], ferrihydrite [$\text{Fe}_5\text{OH}_8 \cdot 4\text{H}_2\text{O}$], schwertmannite [$\text{Fe}_8\text{O}_8(\text{OH})_6\text{SO}_4$], ferro-hexahydrate [$\text{FeSO}_4 \cdot 6\text{H}_2\text{O}$], pentahydrate, siderotil [$\text{FeSO}_4 \cdot 5\text{H}_2\text{O}$], and others belong to this special assembly. Goethite, jarosite and hydrobasaluminite are the most common; the others are less frequent and not stable (Gal 2000).

Minerals occurring in sulfide-rich tailings are:

- Iron oxyhydroxides: goethite, and less frequently lepidocrocite, akageneite, maghemite, ferrihydrite;
- Sulfates: gypsum, bassanite, jarosite, hydrobasaluminite, melanterite, goslarite, ferro-hexahydrate, epsomite, hexahydrate, siderotil, rozenite, anglesite, alunogen, copiapite;
- Clay minerals: vermiculite, mixed-layer mica-vermiculite, smectite, kaolinite;
- Other minerals: marcasite, covellite, sulfur, cristobalite;

Goethite is the most common mineral. It occurs throughout the unsaturated zone, since it is formed either by precipitation from water or by aging from other iron hydroxides. As the iron oxidizes in acid mine waters, the water reaches saturation with

either ferrihydrite or jarosite. Jarosite is a secondary mineral found in the oxidized zones of sulfide deposits forming by the reaction of dilute sulfuric acid in ground water and derived from the oxidation of pyrite. If jarosite weathers or is exposed to dilute waters with higher pH, it gradually decomposes to ferrihydrite or goethite. Jarosite itself is a typical tailings mineral. Its formation probably dates back to the early years of alteration, when large amounts of sulfide minerals were available for oxidation. The decreasing rate of sulfide oxidation results in an observed degree of undersaturation (Germain et al. 1994). This observation is important because hard layers are thought to be important in limiting downward O₂ diffusion. Its color depends upon the iron-to-sulfate ratio. It is reddish brown if the ratio is between 3.5 and 5, and it is canary yellow if the ratio is 1.5. Jarosite formation is connected to the incongruent dissolution of potassium-bearing minerals like biotite, K-feldspar or muscovite.

In a well-formed, mature oxidation profile, there may be a relative decrease in goethite in the surface-leached zone. Intermediate to mature profiles show maximum accumulations at depth, where they form a hardpan layer that marks the zone of higher pH in the profile. The distribution of jarosite is similar to that of goethite with depth, although in a mature profile, jarosite may be absent or scarce in the surface leached zone, but its amount increases with depth, and in the hardpan layer (Gal, 2000). The importance of the hardpan layer lies in its capacity to prevent oxygen diffusion into tailings, thereby limiting further pyrite oxidation. Blowes et al. (1991) characterized two types of hardpan layers. The first type is 10-15 cm thick, occurs 20-30 cm below the depth of active oxidation, and is formed by gypsum and Fe (II) solid phases, principally melanterite. The second type forms at the depth of active oxidation of pyrite, it is 0-5 cm

thick and consists mainly of Fe (III) minerals like goethite, lepidocrocite, ferrihydrite, and jarosite.

Hydrobasaluminite occurs in the weathering zone, usually as a consequence of the oxidation of pyrite and subsequent leaching of clay. It is commonly associated with gypsum, allophane, gibbsite and iron oxides. Hydrobasaluminite can be preserved in the soil matrix indefinitely if kept in contact with moisture (Bannister and Hollingworth 1948), however if hydrobasaluminite forms in a soil profile that has a fluctuating water table, it may dehydrate irreversibly into basaluminite. Hydrobasaluminite has been found to be extremely fine grained and usually mixed with varying amounts of impurities. Hydrobasaluminite was found to occur at a pH of between 4.5 and 5 (Hayden and Rubin 1974).

Because these iron-sulfate hydrate minerals are highly soluble, they provide an instantaneous source of acidic water upon dissolution and hydrolysis. Subsequent oxidation of the ferrous ion, Fe^{+2} , and hydrolysis of the ferric ion, Fe^{+3} , at pH greater than 2 will produce additional acidity (Cravotta 1994). Hence, iron-sulfate hydrate minerals are important as both sinks and sources of AMD by storing acid, Fe, and SO_4^{-2} in a solid phase during dry periods and by releasing the solutes with dissolved during wet periods.

2.5 X-Ray Diffraction

X-Ray Diffraction (XRD) has been used to determine the crystalline structure of clay minerals since the early 1900's. An experiment performed with X-rays established the three prevailing concepts of X-ray diffraction that 1. atomic particles within crystals are arranged in orderly, three-dimensional, repeating patterns; 2. that these regular arrangements have spacings of approximately the same dimensions as the wavelength of

X-rays and therefore, because diffraction does take place, that 3. X-rays are wavelike in nature (Moore and Reynolds 1997). Around the same time, W.L. Bragg discovered the Bragg equation in 1912 (Moore and Reynolds 1997). This equation relates the angle of diffraction with the wavelength and d-spacing or particle width and is stated as

$$2d\sin\Phi = n\lambda \quad [5]$$

where

d = spacing between rows of atoms

Φ = angle of incidence between glass slide and x-ray beam

n = integral number relating to wavelengths

λ = wavelength

These major breakthroughs were the beginning of a century of the study of clay minerals through the use of X-rays. Over the years, the theories and practices of X-ray diffraction have produced numerous diffractograms generated from many naturally occurring clay minerals. In addition to creating diffractograms on real samples, “ideal” diffractograms were created using numerical modeling programs and are now used to identify minerals in natural samples.

2.6 Hydraulic Conductivity-

2.6.1 Grain-Size Predictive Methods

The hydraulic conductivity of sandy aquifers is known to depend both on the matrix and fluid properties of the transmitting medium. The fluid properties, such as density and viscosity, tend to stay constant in most groundwater environments. The shape of the soil particles may vary, depending upon origination point and transportation

history. The smaller the size of the sediment grains, the larger the surface area the water contacts. This increases the frictional resistance to flow, which reduces the intrinsic permeability. For well-sorted sediments, the intrinsic permeability is proportional to the grain size of the sediment (Norris and Fidler 1965).

The porosity depends on the degree of consolidation and cementation of the soil. Rock that comes from the same geologic source would tend to have the same grain shape and porosity factors. In the case of Davis Mine hydrology, the hydraulic conductivity would be dependent on the size of the grains.

Hydraulic conductivity has been related empirically to particle-size distribution by many investigators, e.g., Hazen (1893), Krumbein and Monk (1942), Harleman et al. (1963), Masch and Denny (1966), Alyamani and Sen (1993). Estimation of the hydraulic conductivity of sandy sediments can be done with the Hazen Method (1911), which was originally developed for uniformly graded sand. This method involves the use of the grain-size distribution curve and is applicable to sands where the effective grain size (d_{10}) is between approximately 0.1 and 3.0 mm. The Hazen (1911) approximation is described as

$$K = C_{HAZEN}d_{10}^2 \quad [6]$$

where

- k = Hydraulic Conductivity (cm/sec)
- d_{10} = Effective Grain Size (mm)
- C_{HAZEN} = Coefficient based on the following Table 2.1

Table 2.1: Hazen (1911) Coefficients for Determining Hydraulic Conductivity.

Soil Description	Coefficient, C
Very fine sand, poorly sorted	0.4-0.8
Fine Sand with appreciable fines	0.4-0.8
Medium sand, well sorted	0.8-1.2
Coarse sand, poorly sorted	0.8-1.2
Coarse sand, well sorted, clean	1.2-1.5

The upper and lower bounds seen in the Table 2.1 correspond to the range in coefficients that Hazen (1911) found to occur within a particular sand deposit. In this study, in a well-graded (poorly sorted) medium sand, both the upper and lower bound within Hazen's classification were used to show the range of hydraulic conductivities possible.

Uma et al. (1989) recorreled the aquifer coefficient to a variety of sandy soils. The modified empirical coefficients using the Hazen (1893) equation for hydraulic conductivity are presented in Table 2.2.

Table 2.2: Values for the Uma et al. (1989) Empirical Coefficient

Soil Type	C_{UMA}
Unconsolidated, Poorly Cemented Sands	6
Moderately Consolidated/Cemented Sands or Rock	3.8
Well Compacted and Cemented Sand or Rock	1.2-1.5

Following the work of Hazen, where it was demonstrated that hydraulic conductivity could be related to the square of a characteristic dimension of a sediment, Shepard (1989) analyzed data from eighteen studies where hydraulic conductivity had been related to grain-size distribution. He determined that a general formula could be used to relate all the studies as

$$k = C_{\text{SHEPARD}} d_{50}^j$$

[7]

where

- k = Hydraulic Conductivity (cm/sec)
- d_{50} = Mean Grain Size (mm)
- C_{SHEPARD} = Shape Factor (see Figure 2.3)
- j = Exponent = 1.5-2.0 (see Figure 2.3)

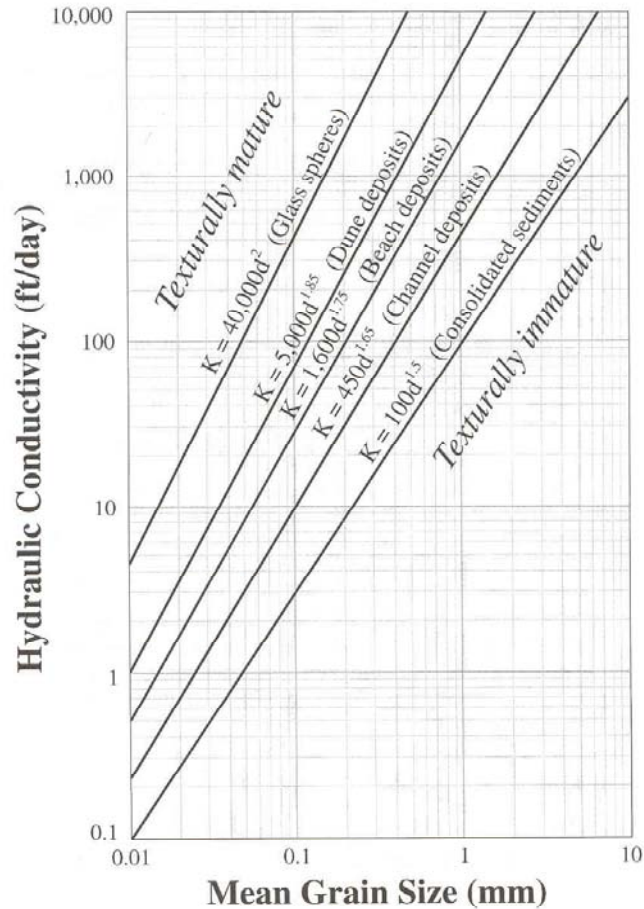


Figure 2.3: Hydraulic Conductivity Relationship to Mean Grain Size (From Shepard 1989)

The data sets that Shepard (1989) produced were used to put together an idealized graph that relates hydraulic conductivity to the mean grain diameter for different sediment types (Figure 2.3).

Beyer determined another correlation in 1964 between grain size and hydraulic conductivity as (found in Vukovic and Soro 1992)

$$k = 0.45 \text{Log} \frac{500}{C_u} d_{10}^2 \quad [8]$$

where

- k = Hydraulic Conductivity (cm/s)
- C_u = Coefficient of Uniformity ($1 < C_u < 20$)
- d_{10} = Grain Size where 10% passes ($0.06 < d_{10} < 0.6$) (mm)

The Beyer formula, contrary to those developed by other authors, does not include the hydraulic conductivity as a function of porosity of the porous media materials.

Other empirical equations relating grain size data to hydraulic conductivity have been developed that include the parameters of shape and packing of the soil grains in which the fluid flows. Hydraulic conductivity is a function of the media and of the fluid in which it flows as stated by Darcy (1856). Darcy's Law is an empirical relationship between velocity and hydraulic gradient and was discovered in 1856 by Henry Darcy that relates these two measurable quantities by a constant of proportionality known as hydraulic conductivity. During experiments performed by Darcy in the laboratory to analyze flow of water through sands, he proposed the empirical law that is now called Darcy's Law as

$$v = -K \left(\frac{dh}{dl} \right) \quad [9]$$

where

- v = Darcy velocity (cm/s)
- dh/dl = hydraulic gradient (m/m)

Hydraulic conductivity is defined as the movement of water through soil that is subject to a gradient driving force. This driving force can be changes in pressure, elevation and or suction per unit distance along the flow path. Hydraulic conductivity is a function of the media in which the fluid is flowing and a function of the fluid itself.

2.6.2 Previous Work – Mine Tailings

Table 2.3 presents the different hydraulic conductivity calculations and their values from the mine tailings area (Gal 2000). Estimates using particle distribution are considered to be less reliable than the results from bail tests, but are good approximations. In the case of some soil samples, the Hazen and Beyer methods were not applicable, because D_{10} , the effective grain size, was greater than 3 mm. Shepard's method is seen to produce the fastest values (average is 2.5×10^{-4} m/s). Hydraulic conductivity calculations with Hvorslev and Bouwer Rice methods give similar values on all cases. The variability in the data suggests that the spoil does not conduct water homogeneously. A hydraulic conductivity of around 10^{-4} m/sec is representative of a fine sand aquifer (Freeze and Cherry 1979). The seismic refraction measurements indicated that the high hydraulic conductivity spoil ($K \sim 10^{-4}$ m/s) is underlain by dense till or weathered bedrock (K is less than 10^{-7} m/s from Freeze and Cherry (1979)), which, in turn, is underlain by the impermeable bedrock (K is less than 10^{-10} m/s from Freeze and Cherry (1979)). This high difference between the spoil and the till prevents acid water from leaking into the bedrock or water from bedrock to the spoil, except in areas where there is a direct contact with fractured bedrock.

Table 2.3: Hydraulic Conductivity Results of the Tailings Pile (after Gal 2000).

Well #	Depth	Grainsize (m/s)			Bail test (m/s)	
		Hazen	Shepard	Beyer	Hvorslev	Bouwer Rice
dmw1	1-50 cm	D ₁₀ >3mm	2.07·10 ⁻⁵	D ₁₀ >3mm		
	50-70 cm	2.46·10 ⁻⁵	1.61·10 ⁻⁴	3.69·10 ⁻⁵	8.76·10 ⁻⁵	4.52·10 ⁻⁵
	70-105 cm	3.28·10 ⁻⁵	2.55·10 ⁻⁴	3.31·10 ⁻⁵		
dmw2	0-30 cm	3.28·10 ⁻⁵	3.79·10 ⁻⁴	3.06·10 ⁻⁵		
	30-40 cm	D ₁₀ >3mm	3.55·10 ⁻⁵	D ₁₀ >3mm		
	pyrite	3.28·10 ⁻⁵	2.18·10 ⁻⁴	3.27·10 ⁻⁵		
dmw3	15-30 cm	D ₁₀ >3mm	1.97·10 ⁻⁵	D ₁₀ >3mm		
	30-50 cm	D ₁₀ >3mm	1.61·10 ⁻⁴	D ₁₀ >3mm		
	50-80 cm	2.46·10 ⁻⁵	1.61·10 ⁻⁴	3.64·10 ⁻⁵		
dmw4	0-15 cm	3.28·10 ⁻⁵	1.86·10 ⁻³	2.45·10 ⁻⁵		
	15-25 cm	3.28·10 ⁻⁵	5.06·10 ⁻⁴	3.06·10 ⁻⁵		
	25-35 cm	3.28·10 ⁻⁵	5.06·10 ⁻⁴	2.95·10 ⁻⁵		
	35-50 cm	3.28·10 ⁻⁵	3.65·10 ⁻⁴	2.95·10 ⁻⁵		
dmw5	0-15 cm	3.28·10 ⁻⁵	4.41·10 ⁻⁴	3.06·10 ⁻⁵	1.18·10 ⁻⁵	7.54·10 ⁻⁶
dmw6	0-5 cm	3.28·10 ⁻⁵	8.81·10 ⁻⁴	2.70·10 ⁻⁵		
	5-15 cm	D ₁₀ >3mm	4.16·10 ⁻⁵	D ₁₀ >3mm		
	15-25 cm	3.28·10 ⁻⁵	1.40·10 ⁻⁴	3.40·10 ⁻⁵		
	25-40 cm	D ₁₀ >3mm	1.66·10 ⁻⁵	D ₁₀ >3mm		
	40-60 cm	D ₁₀ >3mm	2.36·10 ⁻⁵	D ₁₀ >3mm		
	60-80 cm	D ₁₀ >3mm	1.66·10 ⁻⁵	D ₁₀ >3mm		
dmw8	25-70 cm	D ₁₀ >3mm	5.14·10 ⁻⁵	D ₁₀ >3mm	1.34·10 ⁻⁴	6.50·10 ⁻⁵
	70-110 cm	D ₁₀ >3mm	1.97·10 ⁻⁵	D ₁₀ >3mm		
dmw9	25-35 cm	D ₁₀ >3mm	2.26·10 ⁻⁵	D ₁₀ >3mm		
	35-55 cm	D ₁₀ >3mm	1.17·10 ⁻⁵	D ₁₀ >3mm		
	55-65 cm	D ₁₀ >3mm	2.99·10 ⁻⁵	D ₁₀ >3mm		
dmw10	20-40 cm	D ₁₀ >3mm	2.46·10 ⁻⁵	D ₁₀ >3mm		
	40-60 cm	D ₁₀ >3mm	3.55·10 ⁻⁵	D ₁₀ >3mm		
	60-100 cm	D ₁₀ >3mm	2.46·10 ⁻⁵	D ₁₀ >3mm		
dmw11	0-25 cm	3.28·10 ⁻⁵	3.50·10 ⁻⁵	3.06·10 ⁻⁵		
	25-40 cm	1.64·10 ⁻⁵	5.14·10 ⁻⁵	4.06·10 ⁻⁵		
	40-55 cm	3.28·10 ⁻⁵	2.30·10 ⁻⁴	3.08·10 ⁻⁵		
dmw12	10-35 cm	2.46·10 ⁻⁵	8.81·10 ⁻⁴	2.77·10 ⁻⁵	2.07·10 ⁻⁴	1.20·10 ⁻⁴
	35-100 cm	D ₁₀ >3mm	2.46·10 ⁻⁵	D ₁₀ >3mm		
dmw13	0-20 cm	1.64·10 ⁻⁵	1.31·10 ⁻⁴	3.74·10 ⁻⁵		
	20-60 cm	1.64·10 ⁻⁵	6.94·10 ⁻⁵	4.02·10 ⁻⁵		
	60-100 cm	1.60·10 ⁻⁴	6.83·10 ⁻⁴	3.88·10 ⁻⁴		
Average		3.56·10 ⁻⁵	2.46·10 ⁻⁴	5.1·10 ⁻⁵	9.28·10 ⁻⁵	5.85·10 ⁻⁵

3.0 EXPERIMENTAL PROGRAM

Thirty samples were collected at various points throughout the Davis Mine Area in order to best map the mineralogy of the site. The samples were collected with a hand auger. Each hole was drilled until refusal at either bedrock or a layer too difficult to auger through. It was one of the goals of this project to collect samples in profile farther away from the AMD generating area than previous studies, to better understand the weathering processes above bedrock. However, it was extremely difficult to hand auger in certain areas and in other areas there was only a few feet of soil to sample overlying the bedrock. Table 3.1 presents the sample log with soil descriptions and corresponding depths. Figure 3.1 shows the locations of the samples collected. The samples were placed in plastic bags and brought bag to the laboratory, allowed to air dry and then sieved to determine grain-size curves. The soil that passed the 0.075 μm sieve was used to prepare XRD slides.

Table 3.1: Soil Sample Log and Soil Descriptions

Sample #	Sample ID	Depth (m)	Soil Description
1	Well 6	0.30	brownish-red silty/clay
2	Well 7	0.30	grey silty sand, some gravel
3	"	0.61	pyrite flecks, silty sand cobbles, grey
4	"	0.91	change from grey silt to brown clayey silt
5	"	0.99	red clay
6	"	1.07	red clay
7	"	1.22	red clay
8	"	1.52	red clay (hit water table 58"-refusal 66")
9	Hole A	0.30	yellowish brown mottled
10	"	0.61	greenish brown silty soil with gravel
11	02-01	Surface	Grab Samples
12	02-03	Surface	Grab Samples
13	02-07	Surface	Grab Samples
14	02-09	Surface	Grab Samples
15	02-10	Surface	Grab Samples
16	Hole B	0.30	yellowish brown mottled
17	Hole C	0.30	greyish silty clay
18	"	0.61	greyish silty clay
19	"	0.76	yellow, sulfur chunks
20	"	0.91	yellow with greyish flecks
21	"	1.22	yellow silt with sand
22	"	1.52	yellow clayey with weathered rock chunks - Refusal 65"
23	Hole D	0.30	brown silty sand
24	"	0.61	reddish brown clayey soil
25	Well 9	0.30	brown silty soil
26	"	0.61	yellow, brown mottled with sulfur chunks; friable
27	"	0.91	red clay
28	"	1.22	sandy red silt with grey flecks (refusal 57")
29	Well 5	0.61	Spoon Sample
30	Well 2	0.61	Spoon Sample

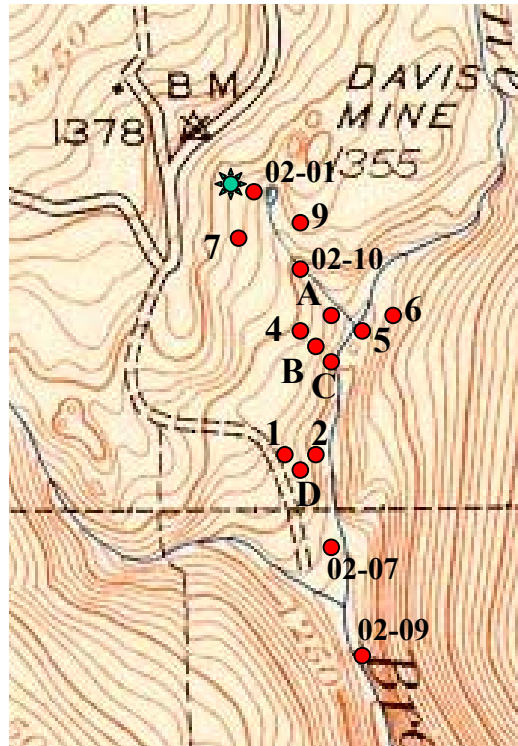


Figure 3.1: Location Map of Soil Samples.

3.1 Grain-Size Analysis

The Sieve Analysis was performed in general accordance with American Society for Testing and Materials (ASTM) D 422 – 63 Standard Test Method for *Particle-Size Analysis of Soils* (ASTM 1998).

For coarse-grained soils, a sieve analysis is performed in which a sample of dry soil is shaken mechanically through a series of woven-wire square-mesh sieves with successively smaller openings. Eight wire-mesh sieves were assembled in the following order: 9.5-mm (3/8”), #4, #10, #20, #40, #60, #100, and #200 plus the pan that would catch the soil finer than the #200 sieve. Each sieve was cleaned and weighed. Approximately 500 grams of sample was poured into the top of the sieve stack. A top

was placed on the 9.5-mm sieve and the stack was placed in the mechanical shaker for 10 minutes. After the mechanical shaker stopped, the sieves were carefully pulled apart, taking care not to spill any soil. The sieves were weighed with the soil and recorded. The soil that passed the #200 sieve (0.075 μm) was saved and used in the sample preparation for the X-Ray Diffraction testing.

3.2 XRD Sample Preparation

All of the samples in this project were prepared using a qualitative analysis of clay minerals. Approximately five (5) to ten (10) grams of soil that passed the #200 sieve were placed into a centrifuge bottle. The bottles were placed on a shaker table, then sonified in an ultrasonic dismembrator and then placed in the IEC-UV centrifuge for 9 minutes and 37 seconds at 500 rpm to separate out the $>2\mu\text{m}$ size fraction. Once this was accomplished, the clay suspension was decanted into a high speed centrifuge bottle and the sample was again centrifuged at 10,000 RPM for 30 minutes. The clear liquid was removed and the remaining sediment was mixed into a slurry and used to prepare x-ray slides. Oriented slides were prepared using the glass slide method.

3.2.1 Slide Treatments

Once the slides were prepared using the glass slide method, and the diffractograms were analyzed, it was decided to perform one additional treatment on six samples because of the existence of a d spacing of around 12, a typical value for smectite;

Well 6-1', Well 7 - 5', Well 9 - 3 and 4', Well 5 - 2' and Well 2 - 2'. The slides were treated by ethylene glycol solvation and placed in a desiccator on a platform above the ethylene glycol so as to not allow the slides contact with the liquid glycol. The desiccator was then placed in an oven at 60 °C. The slides were exposed to the vapor for twenty-four (24) hours. The analysis of these samples were performed immediately so that the ethylene glycol would not evaporate

3.2.3 Diffractogram Generation

The X-ray diffraction program was performed using a Siemens K4 generator (1978) with a Type F goniometer. The data was processed with a Databox digital system (1991). The X-ray generator used 45 kV and 20 mA to generate Cu-K alpha (Copper K-alpha) radiation. A computer program named "TALK" controlled the goniometer. The goniometer was calibrated using a maximum stepping rate of 350 Hz, minimum and maximum angles of 2 and 130 respectively, number of steps, 400, and backlash compensation of 0.018. The information required for the goniometer to perform the analysis was an initial and final angle (2 and 30 degrees respectively for oriented mounts). The goniometer also required a step size and duration for each count. The step size values used in this analysis was 0.05° and the count duration was 1 second for oriented slides. The glass slide was placed in the sample holder and the X-ray diffractograms were generated.

4.0 RESULTS

4.1 Grain-Size Analysis

Tables 4.1 and 4.2 present the results of the grain-size distribution tests and the hydraulic conductivity estimates based on three predictive methods, Hazen (1911), Shepard (1989) and Beyer (1964). The overall average hydraulic conductivities of the site are Lower Hazen, 2.0×10^{-4} m/s (55 ft/day), Upper Hazen 3.0×10^{-4} m/s (83 ft/day), Shepard 1.5×10^{-4} m/s (42 ft/day) and Beyer 2.0×10^{-4} m/s (62 ft/day). Well profile averages are shown in Table 4.3. The Hazen and Beyer methods use d_{10} values and the Shepard Method utilizes the d_{50} value. The grain-size distribution data sheets are presented in Appendix A.

Table 4.1: Grain-Size Distribution Results.

Sample #	Sample ID	Depth (m)	d ₁₀ (mm)	d ₃₀ (mm)	d ₅₀ (mm)	d ₆₀ (mm)	C _u		C _c
1	Well 6	0.30	0.08	0.22	0.65	1.10	13.75	Poorly Sorted	0.55
2	Well 7	0.30	0.16	0.40	0.80	1.30	8.13	Poorly Sorted	0.77
3	"	0.61	0.08	0.29	0.58	0.78	9.75	Poorly Sorted	1.35
4	"	0.91	0.14	0.24	0.50	0.70	5.00	Poorly Sorted	0.59
5	"	0.99	0.16	0.30	0.60	0.90	5.63	Poorly Sorted	0.63
6	"	1.07	-	0.12	0.28	0.50	-		-
7	"	1.22	-	0.09	0.16	0.22	-		-
8	"	1.52	-	0.15	0.40	0.70	-		-
9	Hole A	0.30	0.19	0.27	0.80	1.30	6.84	Poorly Sorted	0.30
10	"	0.61	0.30	0.50	0.90	1.50	5.00	Poorly Sorted	0.56
11	02-01	Surface	0.08	0.17	0.36	0.58	7.25	Poorly Sorted	0.62
12	02-03	Surface	0.18	0.40	0.80	1.30	7.22	Poorly Sorted	0.68
13	02-07	Surface	0.09	0.17	0.24	0.35	3.89	Well Sorted	0.92
14	02-09	Surface	-	-	-	-	-		-
15	02-10	Surface	0.14	0.30	0.54	0.70	5.00	Poorly Sorted	0.92
16	Hole B	0.30	0.14	0.28	0.55	0.85	6.07	Poorly Sorted	0.66
17	Hole C	0.30	0.11	0.26	0.57	0.95	8.64	Poorly Sorted	0.65
18	"	0.61	0.15	0.30	0.70	1.30	8.67	Poorly Sorted	0.46
19	"	0.76	0.09	0.25	0.60	0.95	10.56	Poorly Sorted	0.73
20	"	0.91	0.25	0.33	0.50	0.60	2.40	Well Sorted	0.73
21	"	1.22	0.27	0.40	0.75	1.10	4.07	Well Sorted	0.54
22	"	1.52	0.18	0.30	0.40	0.56	3.11	Well Sorted	0.89
23	Hole D	0.30	0.09	0.21	0.47	0.77	8.56	Poorly Sorted	0.64
24	"	0.61	-	0.10	0.20	0.25	-		-
25	Well 9	0.30	0.13	0.27	0.60	1.20	9.23	Poorly Sorted	0.47
26	"	0.61	0.13	0.29	0.70	1.20	9.23	Poorly Sorted	0.54
27	"	0.91	0.07	0.23	0.65	0.97	13.86	Poorly Sorted	0.78
28	"	1.22	-	0.15	0.60	1.40	-		-
29	Well 5	0.61	0.10	0.20	0.40	0.57	6.00	Poorly Sorted	0.74
30	Well 2	0.61	-	0.16	0.40	0.70	-		-

Table 4.2: Hydraulic Conductivity Predictive Method Results.

Sample #	Sample ID	Depth (m)	Lower	Upper	Shephard	Beyer
			Hazen Method k (m/s)	Hazen Method k (m/s)		
1	Well 6	0.30	5.11E-05	7.66E-05	1.84E-04	4.49E-05
2	Well 7	0.30	2.04E-04	3.07E-04	2.52E-04	2.06E-04
3	"	0.61	5.11E-05	7.66E-05	1.55E-04	4.91E-05
4	"	0.91	1.56E-04	2.35E-04	1.24E-04	1.76E-04
5	"	0.99	2.04E-04	3.07E-04	1.64E-04	2.24E-04
6	"	1.07	D ₁₀ >3mm	D ₁₀ >3mm	5.22E-05	D ₁₀ >3mm
7	"	1.22	D ₁₀ >3mm	D ₁₀ >3mm	2.25E-05	D ₁₀ >3mm
8	"	1.52	D ₁₀ >3mm	D ₁₀ >3mm	8.90E-05	D ₁₀ >3mm
9	Hole A	0.30	2.88E-04	4.32E-04	2.52E-04	3.02E-04
10	"	0.61	7.19E-04	1.08E-03	3.01E-04	8.08E-04
11	02-01	Surface	5.11E-05	7.66E-05	7.60E-05	5.28E-05
12	02-03	Surface	2.59E-04	3.88E-04	2.52E-04	2.68E-04
13	02-07	Surface	6.47E-05	9.70E-05	4.14E-05	7.67E-05
14	02-09	Surface	NA	NA	NA	NA
15	02-10	Surface	1.56E-04	2.35E-04	1.40E-04	1.76E-04
16	Hole B	0.30	1.56E-04	2.35E-04	1.44E-04	1.69E-04
17	Hole C	0.30	9.66E-05	1.45E-04	1.51E-04	9.58E-05
18	"	0.61	1.80E-04	2.69E-04	2.06E-04	1.78E-04
19	"	0.76	6.47E-05	9.70E-05	1.64E-04	6.09E-05
20	"	0.91	4.99E-04	7.48E-04	1.24E-04	6.51E-04
21	"	1.22	5.82E-04	8.73E-04	2.29E-04	6.84E-04
22	"	1.52	2.59E-04	3.88E-04	8.90E-05	3.21E-04
23	Hole D	0.30	6.47E-05	9.70E-05	1.13E-04	6.43E-05
24	"	0.61	D ₁₀ >3mm	D ₁₀ >3mm	3.15E-05	D ₁₀ >3mm
25	Well 9	0.30	1.35E-04	2.02E-04	1.64E-04	1.32E-04
26	"	0.61	1.35E-04	2.02E-04	2.06E-04	1.32E-04
27	"	0.91	3.91E-05	5.87E-05	1.84E-04	3.43E-05
28	"	1.22	D ₁₀ >3mm	D ₁₀ >3mm	1.64E-04	D ₁₀ >3mm
29	Well 5	0.61	7.20E-05	1.08E-04	8.90E-05	7.78E-05
30	Well 2	0.61	D ₁₀ >3mm	D ₁₀ >3mm	8.90E-05	D ₁₀ >3mm

Table 4.3: Average Hydraulic Conductivity Values in Well Profiles.

	Lower Hazen Method k (m/s)	Upper Hazen Method k (m/s)	Shephard k (m/s)	Beyer k (m/s)
Hole A	5.03E-04	7.55E-04	2.76E-04	5.55E-04
Hole C	2.80E-04	4.20E-04	1.61E-04	3.32E-04
Hole D	6.34E-05	9.86E-05	1.13E-04	6.34E-05
Well 7	1.54E-04	2.31E-04	1.23E-04	1.64E-04
Well 9	1.03E-04	1.54E-04	1.79E-04	9.91E-05

4.2 XRD Analysis

The results of the X-Ray Diffraction tests performed on each sample are shown below. The mineral contents in the clay fraction of the samples are presented in Table 4.4. The diffractograms are presented in the order of Table 4.4. The most common clay minerals present in these thirty representative samples are chlorite and illite with some samples containing a kind of smectite. Most of the samples contain a potassium iron sulfate hydroxide called jarosite. Jarosite is a product of sulfide oxidations, which is abundant throughout the site. This jarosite is found in varying quantities depending on the depth of the sample and is found to be present in layers throughout the site.

The most common d-spacings found in this study are summarized in Table 4.5 and Table 4.6. These peaks were found in multiple samples and are typical peaks for the associated clay minerals or non-clay components. Full size diffractograms are presented in Appendix B.

Table 4.4: Mineral Contents in the Clay Fraction of the samples by XRD Analysis.

Sample #	Sample ID	Depth (m)	Contents	
1	Well 6	0.30	Chlorite, Smectite, Illite, Quartz and Apatite	
2		0.30	Illite, Chlorite, Jarosite, Quartz and Feldspar	
3		0.61	Illite, Jarosite, Quartz and Feldspar	
4		0.91	Chlorite, Jarosite, Quartz	
5	Well 7	0.99	Jarosite	
6		1.07	Chlorite, Illite, Quartz and Apatite	
7		1.22	Chlorite, Illite, Quartz, Feldspar and Apatite	
8		1.52	Chlorite, Smectite, Illite, Jarosite, Quartz and Feldspar	
9	Hole A	0.30	Chlorite, Illite, Jarosite, Quartz and Feldspar	
10		0.61	Chlorite, Illite, Jarosite and Quartz	
11	02-01	Surface	Chlorite, Illite, Jarosite, Quartz and Feldspar	
12	02-03	Surface	Illite and Jarosite	
13	02-07	Surface	Chlorite, Illite, Jarosite, Quartz and Feldspar	
14	02-09	Surface	Jarosite, Quartz and Feldspar	
15	02-10	Surface	Chlorite, Illite, Jarosite, Quartz and Feldspar	
16	Hole B	0.30	Jarosite	
17		0.30	Jarosite	
18		0.61	Jarosite	
19		Hole C	0.76	Chlorite, Illite, Jarosite, Quartz and Feldspar
20			0.91	Chlorite, Illite, Jarosite, Quartz and Feldspar
21			1.22	Chlorite, Illite, Jarosite, Quartz and Feldspar
22	1.52		Chlorite, Illite, Jarosite and Quartz	
23	Hole D	0.30	Chlorite, Illite, Jarosite and Quartz	
24		0.61	Chlorite, Illite, Quartz and Feldspar	
25	Well 9	0.30	Chlorite, Jarosite and Quartz	
26		0.61	Illite, Jarosite and Quartz	
27		0.91	Chlorite, Smectite?, Jarosite, Quartz and Feldspar	
28		1.22	Chlorite, Smectite, Jarosite and Quartz	
29	Well 5	0.61	Chlorite, Smectite, Illite, Jarosite and Quartz	
30	Well 2	0.61	Chlorite, Smectite, Illite, Quartz and Feldspar	

Table 4.5: Common d-Spacings in Å for Typical Clay Minerals.

Reflections	Chlorite	Smectite	Illite	Kaolinite
(001)	14.2	12.2	10.0	7.0
(002)	7.1	6.1	5.0	3.5
(003)	4.7	4.1	3.3	
(004)	3.6	3.1		

Table 4.6: Common d-Spacings in Å for Typical Non-Clay Components.

Jarosite	Hydrobasaluminite	Feldspar	Quartz	Barite	Gibbsite
5.90	12.60	3.18-3.21	4.24	3.12	3.2
5.73	6.3		3.34		
5.08	4.2				
3.65	4.0				
3.08	3.15				

4.2.1 Air-Dried Oriented Glass Slide

Figure 4.1 presents the diffractogram for Well 6 at one foot below the surface. This trace shows a definite (001) chlorite peak at a d spacing of approximately 14.3, a (002) peak at 7.1, a (003) peak at 4.7 and a (004) peak at 3.5. This diffractogram also shows the presence of hydrobasaluminite at approximately 12.5 and at 6.25. Hydrobasaluminite is an aluminum iron sulfate hydroxide that is a precursor to the mineral basaluminite. Illite can also be seen in this trace with an (001) peak around a d spacing of 10, (002) at 4.9 and a strong (003) peak at 3.33, along with probably some quartz as well and at a d spacing of 4.22. The peak at a d spacing of 3.12 could indicate a sulfate such as barite, which is known to exist on this site.

Figure 4.2 presents the results of the XRD process on a sample from Well 7 at one foot below the surface. This sample looks to contain some sort of mixed layer minerals, maybe including chlorite, even though there is no real peak, just a shoulder. The possibility for chlorite lies in a small (002 and(003) peaks at 7 and 3.75 respectively. There is a strong illite (001) peak at about d=10 as well as a (002) and a (003) illite peak present. Quartz is again present at d = 4.24 and 3.3 mixed in with the illite (003) signal.

There seems to be some jarosite present in this sample with peaks at $d = 5.7, 3.65$ and 3.08 . A feldspar peak is present at $d = 3.18$.

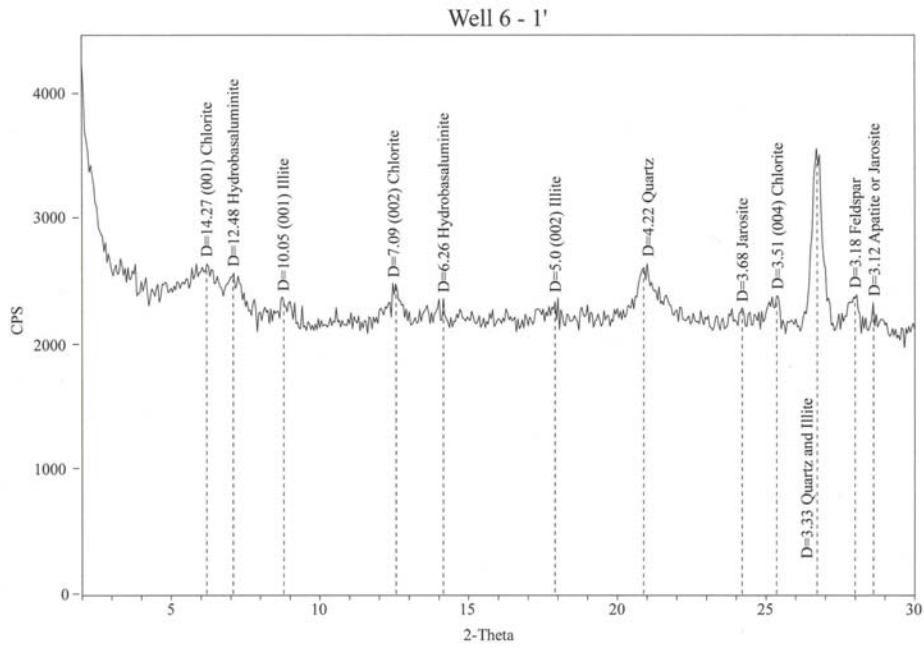


Figure 4.1: Diffractogram for Well 6 – 1’.

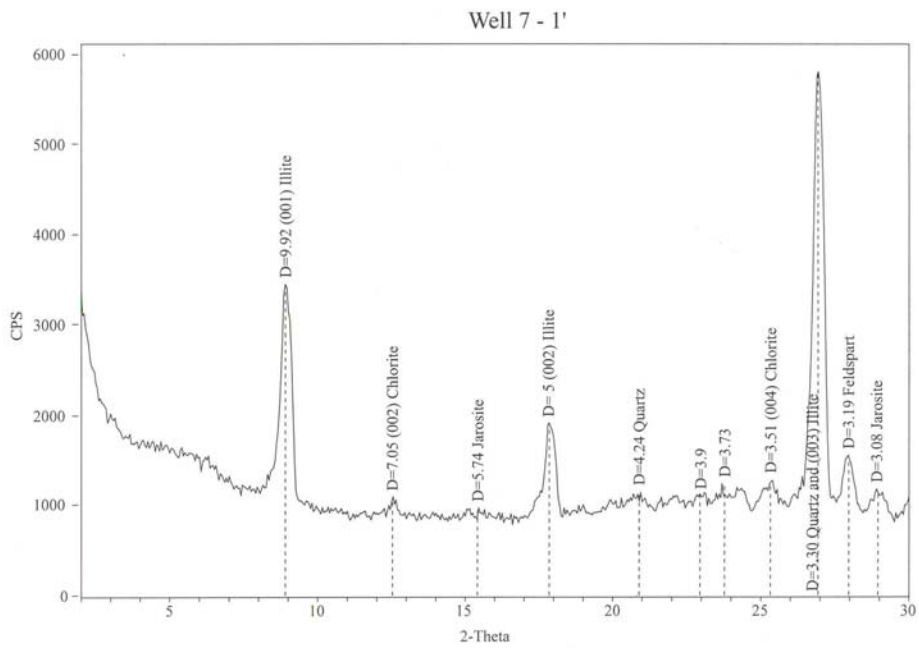


Figure 4.2: Diffractogram for Well 7-1’.

Figure 4.3 presents the results of Well 7 at two feet below the surface. There is a small Illite (001) peak around $d = 10$ and a (002) and (003) peak. Feldspar may be present in this sample at $d = 3.19$ and jarosite may be in this sample as well with peaks shown at $d = 5.08$ and 3.08 . Hydrobasaluminite may be present with a peak at 6.27 . There are a number of very miniscule peaks that may just be background.

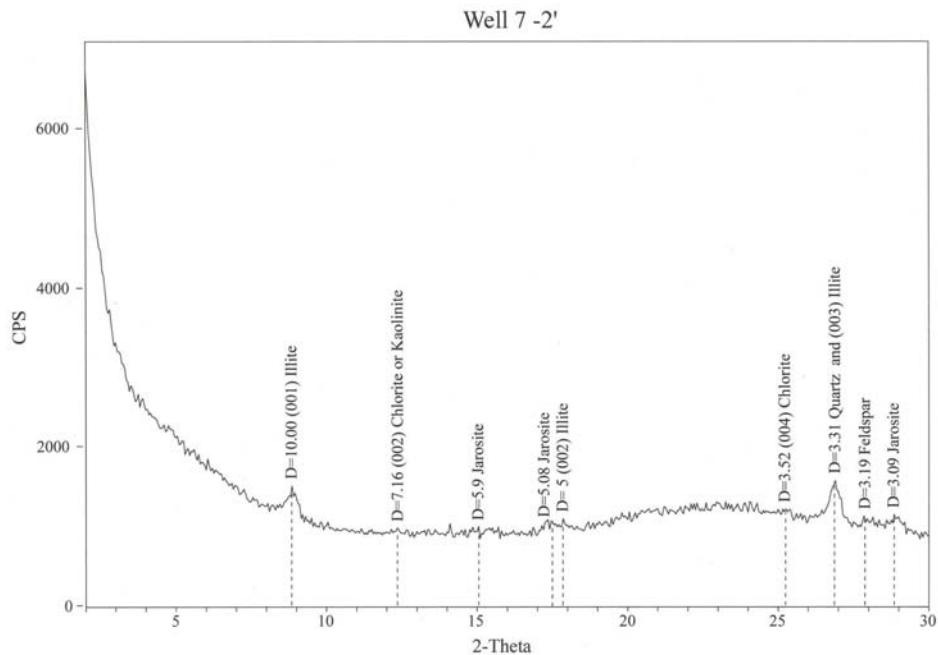


Figure 4.3: Diffractogram for Well 7-2'.

Results of XRD testing on Well 7 at three feet below the surface is presented in Figure 4.4. At this depth, there is a clearer chlorite (001) peak, as well as a (002) and (004) peak. There may be some illite and some hydrobasaluminite in this sample and there is quartz present at the two typical peaks of $d = 4.24$ and 3.34 . The most striking peaks on this diffractogram come from the sulfate, jarosite, with very definitive peaks at $d = 5.7$, 5.1 , 3.65 and 3.08 . The jarosite was not really present in the first two feet of this profile, but by the third foot, it really stands out as the dominant component.

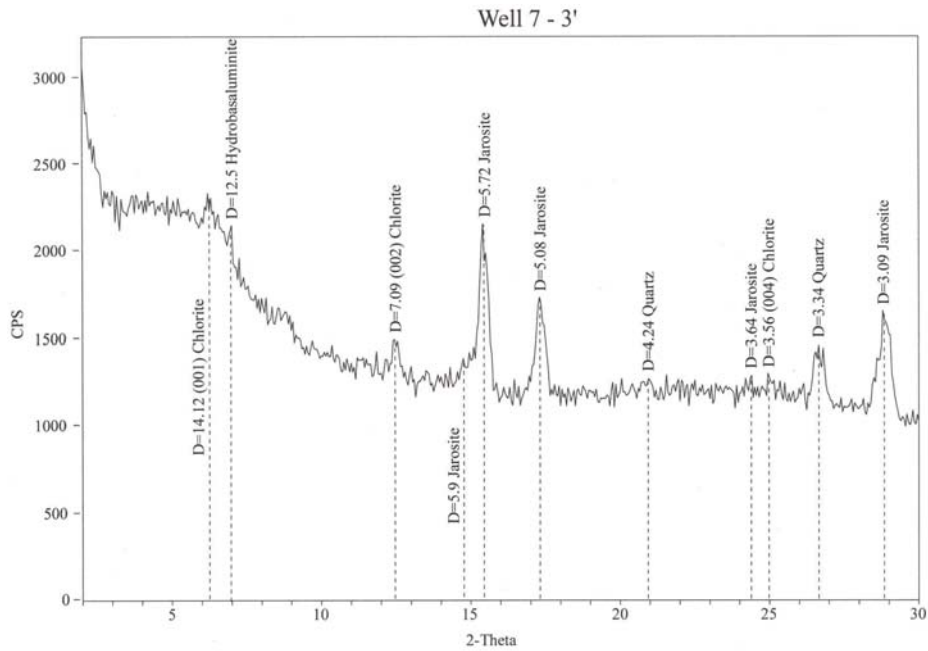


Figure 4.4: Diffractogram for Well 7-3'.

The results of Well 7 at 3.25 feet are presented in Figure 4.5. Again, as in the three foot sample results, the diffractogram shows a poorly crystalline interlayered clay with strong jarosite peaks at $d = 5.7, 5.09$ and 3.09 .

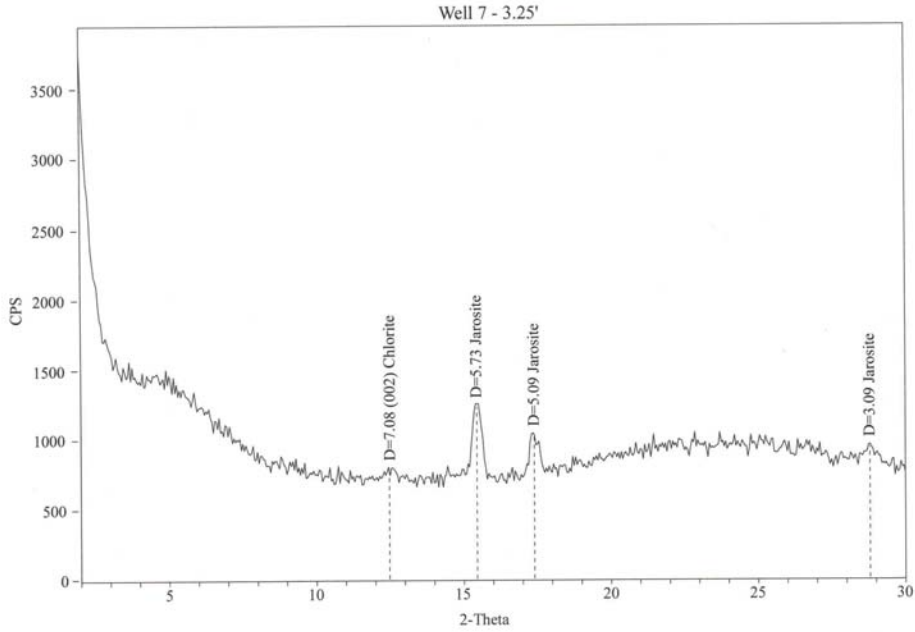


Figure 4.5: Diffractogram for Well 7-3.25'.

Well 7, 3.5 feet, (Figure 4.6), shows a strong chlorite (001), (002), (003) and (004) peaks. There is also some illite (001), (002), (003). A feldspar peak is seen at d = 3.18 and there is a possible jarosite peak at 3.09.

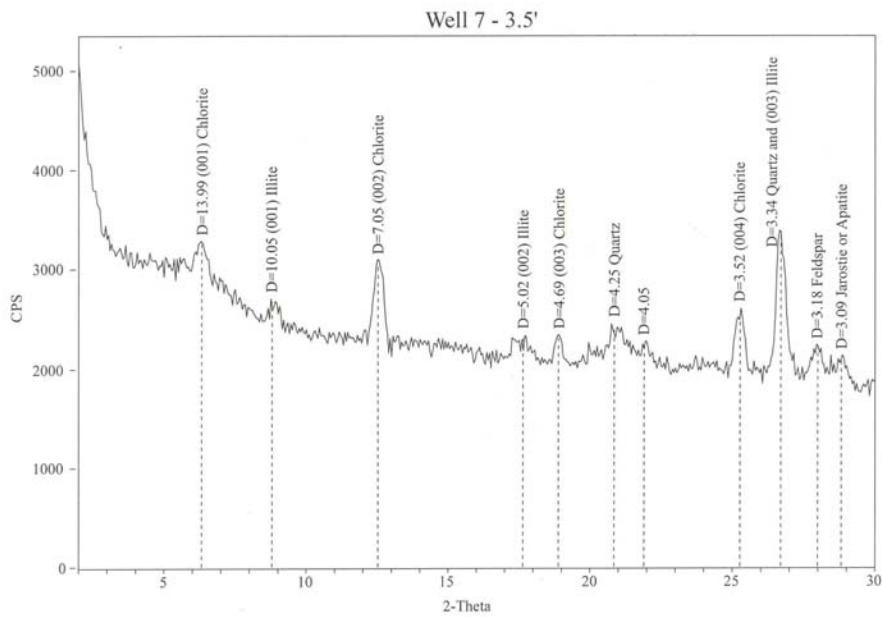


Figure 4.6: Diffractogram for Well 7-3.5'.

Figure 4.7 shows the results of Well 7, at four feet. There are chlorite (001), (002), (003) and (004) peaks and illite (001), (002) and (003) peaks present. Quartz peaks can

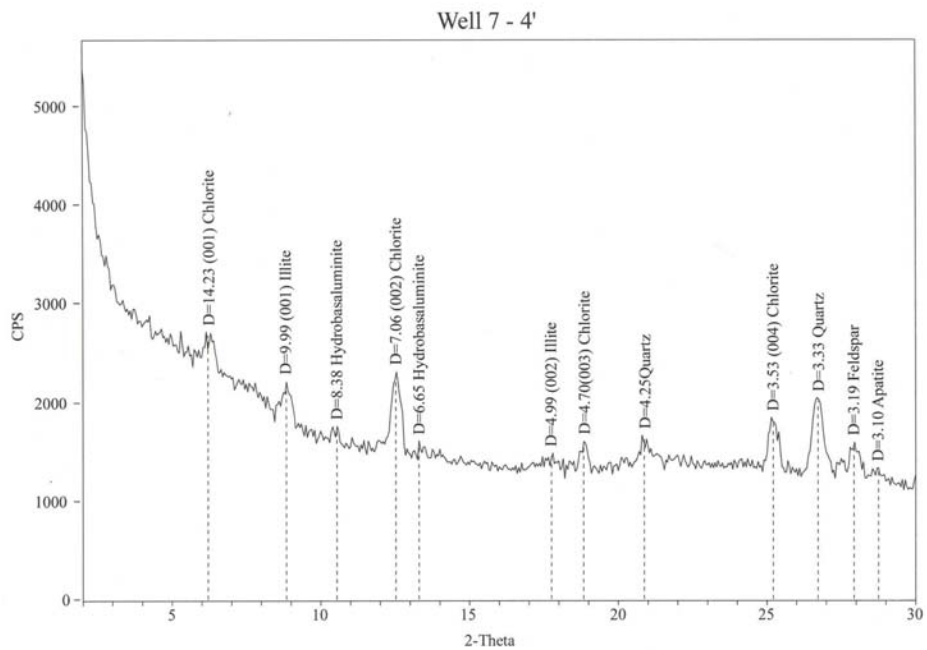


Figure 4.7: Diffractogram for Well 7-4'.

be seen at $d = 4.25$ and mixed in with the illite (003) peak at $d = 3.33$. There seems to be some feldspar and maybe some jarosite with only one peak at $d = 3.1$.

Figure 4.8 presents the diffractogram of Well 7, five feet. There are distinctive chlorite and illite peaks along with the aluminum iron sulfate hydroxide, hydrobasaluminite a 12 \AA peak. Again, there may be some feldspar and jarosite.

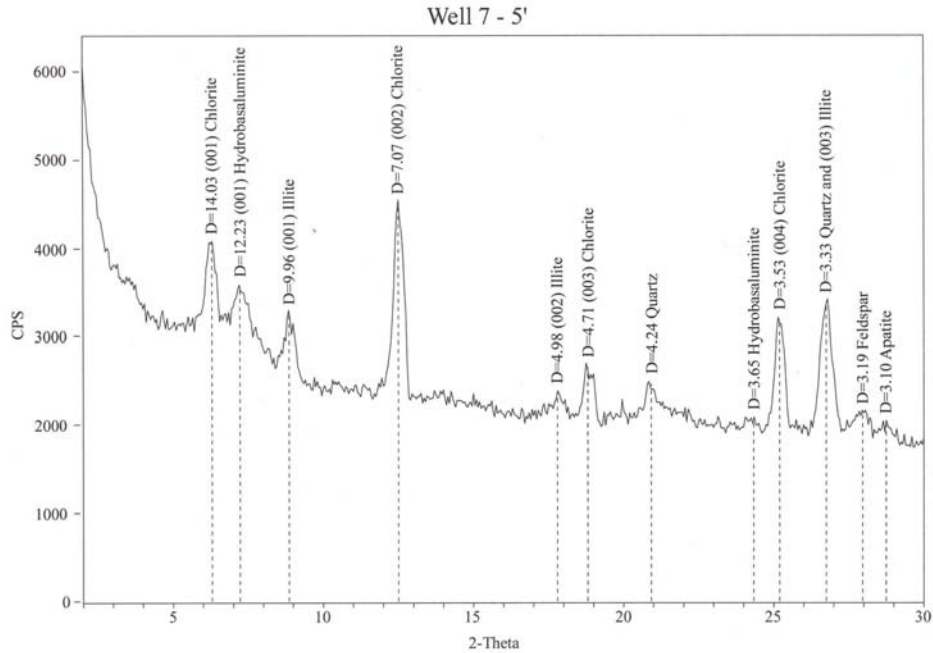


Figure 4.8: Diffractogram for Well 7-5'.

Figure 4.9 presents the diffractogram for Hole A, one-foot. This sample is extremely crystalline with sharp peaks of chlorite (001), (002), (003), (004) and illite (001),(002) and (003). This sample also contains the peaks of jarosite at $d = 5.9, 5.7, 5.08, 3.65$ and a big peak at 3.08 . There is a peak at around 11 \AA that may be aluminum iron sulfate hydroxide, hydrobasaluminite, or another iron sulfate hydroxide formed from pyrite oxidation. Figure 4.10 presents the diffractogram for Hole A, two feet. As seen in the shallower sample in this hole, the sample contains chlorite and illite and also the same peaks of jarosite, however, the clay mineral peaks in this sample are not as intense as in the one-foot sample.

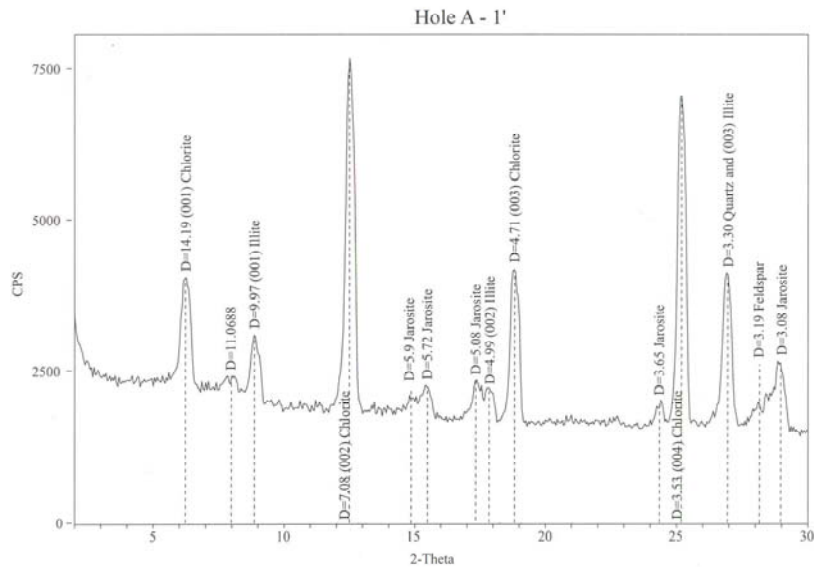


Figure 4.9: Diffractogram for Hole A – 1’.

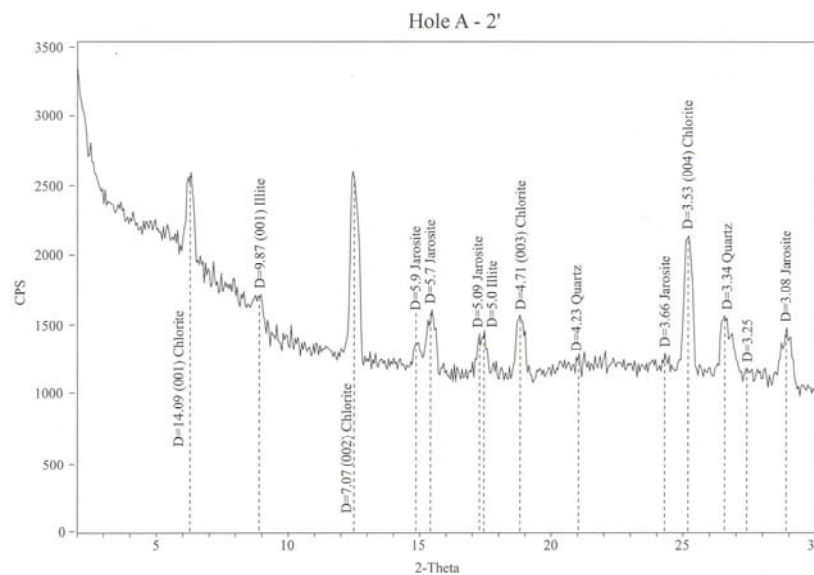


Figure 4.10: Diffractogram for Hole A – 2’.

Sample 02-01 was a grab sample taken from about 0.5 feet below the surface in the dry channel about 10 yards from the Mine Shaft #1. The diffractogram shows that it has a regular pattern of chlorite and illite with the now familiar jarosite peaks. Feldspar and quartz are also present in this sample (Figure 4.11).

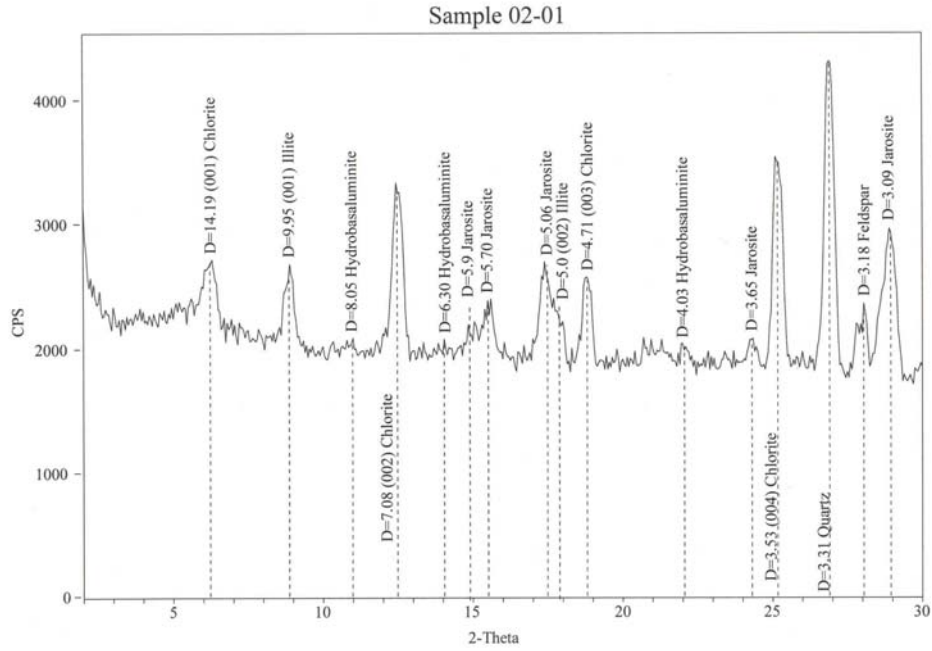


Figure 4.11: Diffractogram for Sample 02-01.

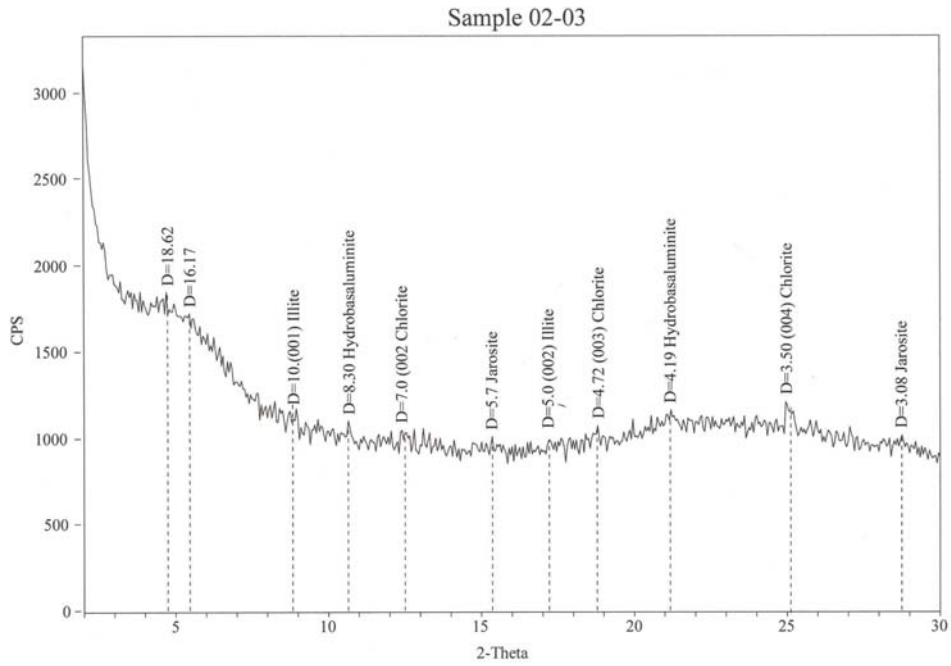


Figure 4.12: Diffractogram for Sample 02-03.

Figure 4.12 presents the diffractogram of grab Sample 02-03. This sample did not contain much clay and the diffractogram does not show many strong clay mineral peaks, but rather a typical diffractogram of a glass slide.

Sample 02-07 was another grab sample taken by Well #2 on the bank. This sample shows some chlorite and illite peaks as well as jarosite, feldspar and quartz (Figure 4.13)

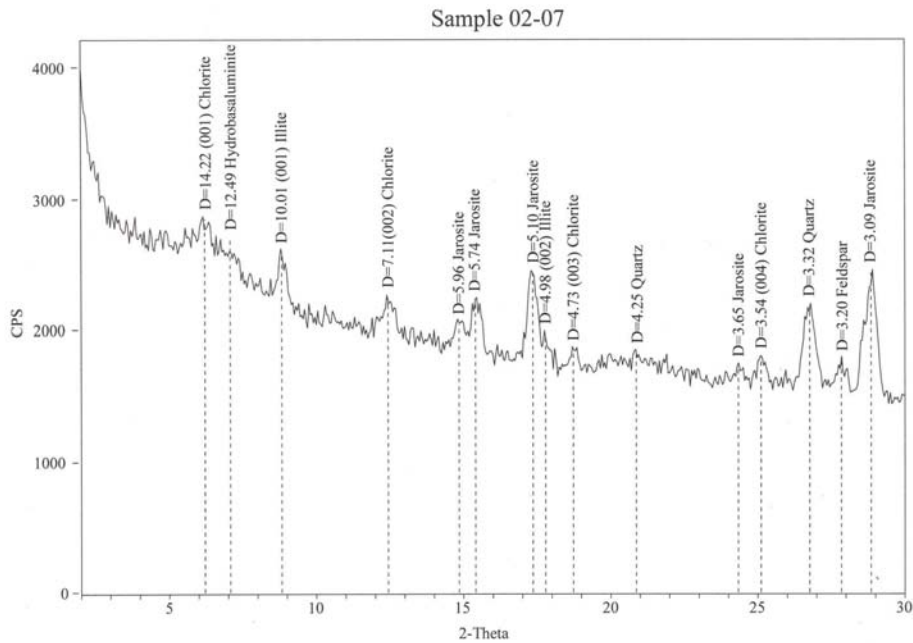


Figure 4.13: Diffractogram for Sample 02-07.

Sample 02-09 was a grab sample from the powerlines downstream of the site. This diffractogram had a little more background noise in it and the peaks were not that clear. Jarosite seems to be the dominant component of this sample. The sample also contains quartz and feldspar and hydrobasaluminite. It is possible that there are some weak chlorite crystals in the sample as well (Figure 4.14).

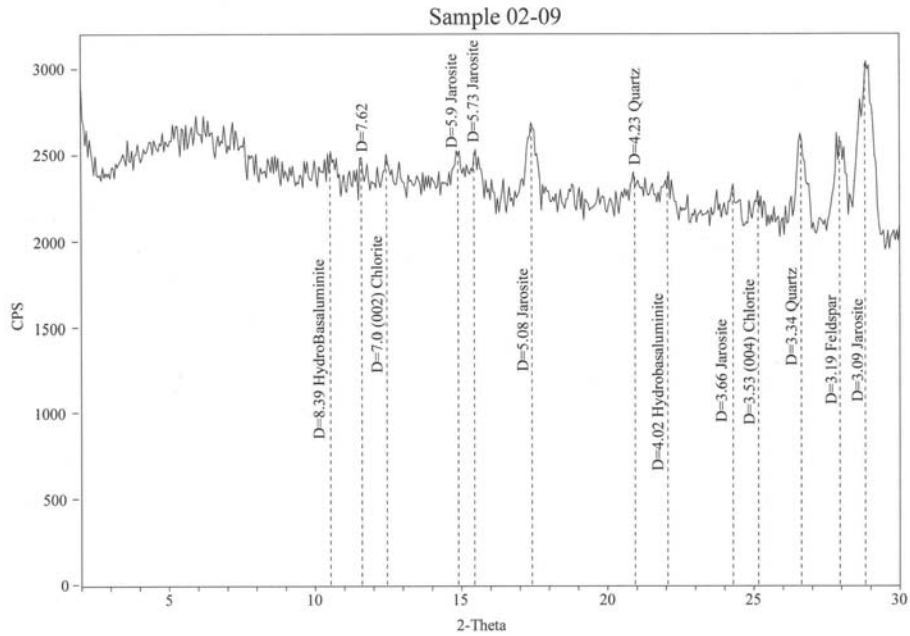


Figure 4.14: Diffractogram for Sample 02-09.

Sample 02-10 was a grab sample from a tailings pile in the middle of the site in the stream channel. There seems to be some mixed clay minerals in this sample with some definite chlorite/illite clay minerals along with jarosite, feldspar and quartz (Figure 4.15).

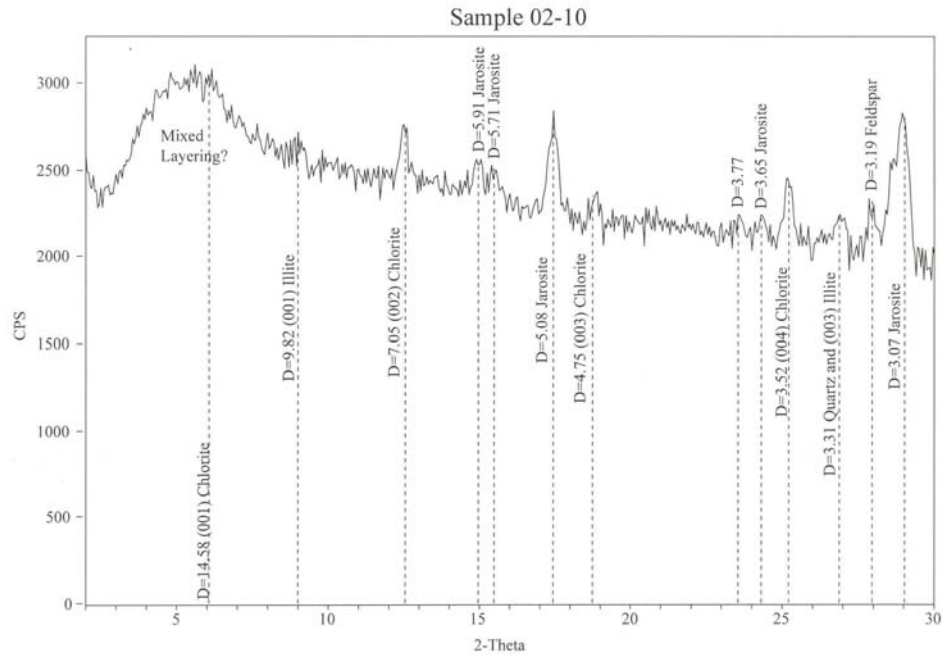


Figure 4.15: Diffractogram for Sample 02-10.

Hole B, one-foot sample, was taken from between Wells 4 and 3 on the edge of the old logging road nearer the stream. This soil shows no clay minerals. The only peaks that can be seen on this diffractogram are jarosite. Unfortunately, hand augering was halted by a large rock in this hole and only one sample was collected from this location (Figure 4.16).

Hole C was augered fifteen feet from Hole B, closer to well 3, on top of the tailings pile. This diffractogram shows some small, not well-defined chlorite peaks and very distinctive jarosite peaks at $d = 5.9, 5.7, 5.1, 3.65$ and 3.08 (Figure 4.17). The two-foot sample in Hole C is similar to the one-foot sample. There are five distinctive jarosite peaks and not many clay minerals (Figure 4.18). The 2.5-foot sample shows some chlorite and illite peaks along with an abundance of jarosite. Feldspar and quartz are also

present (Figure 4.19). There are three distinctive peaks of hydrobasaluminite at $d = 6.4$, 4.02 and 3.75.

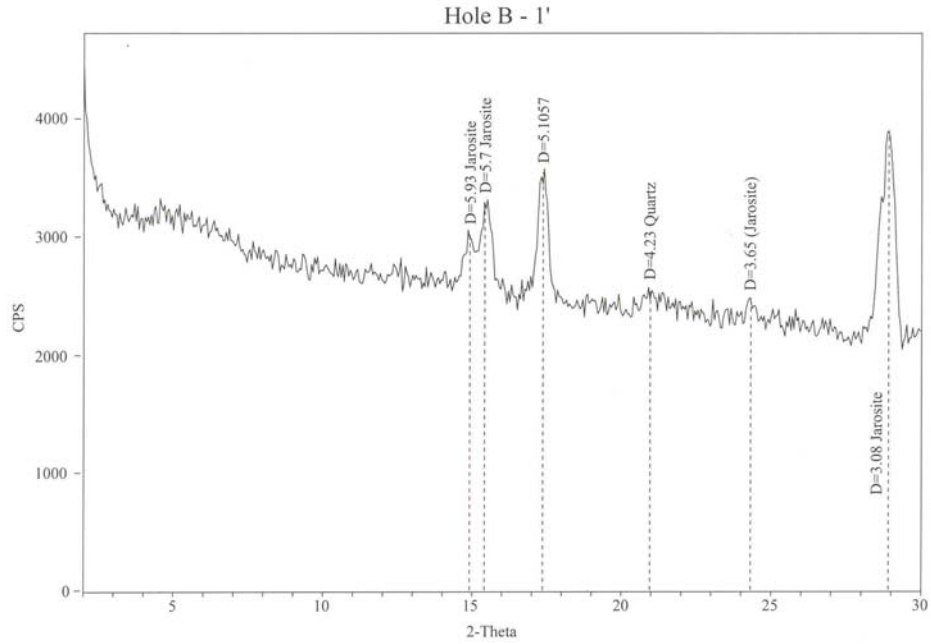


Figure 4.16: Diffractogram for Hole B – 1’.

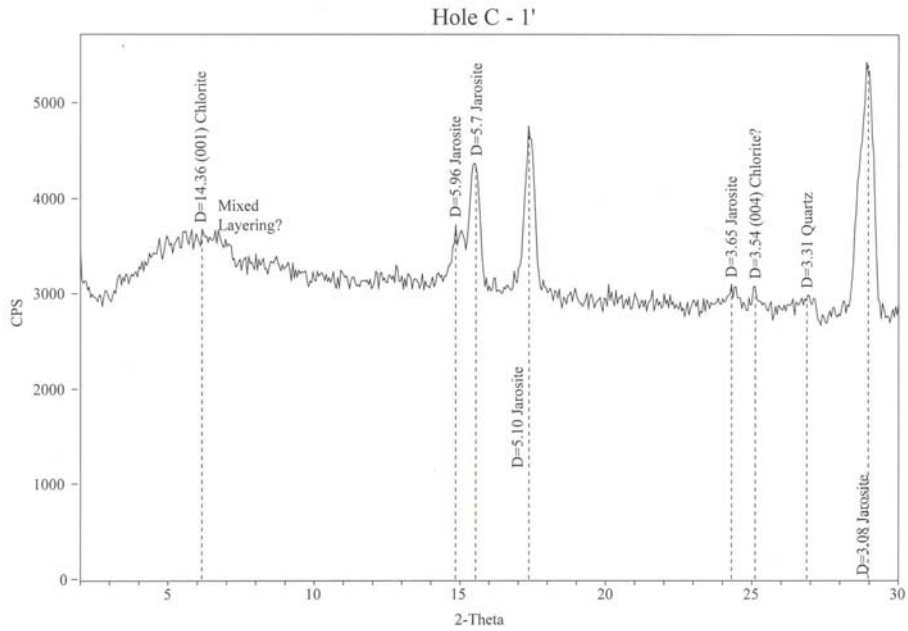


Figure 4.17: Diffractogram for Hole C – 1’.

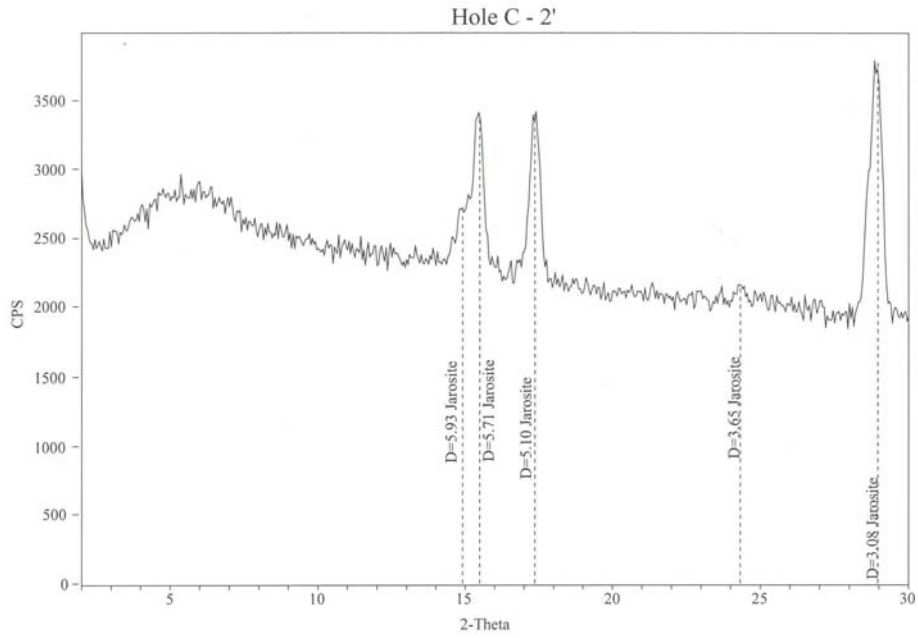


Figure 4.18: Diffractogram for Hole C – 2'.

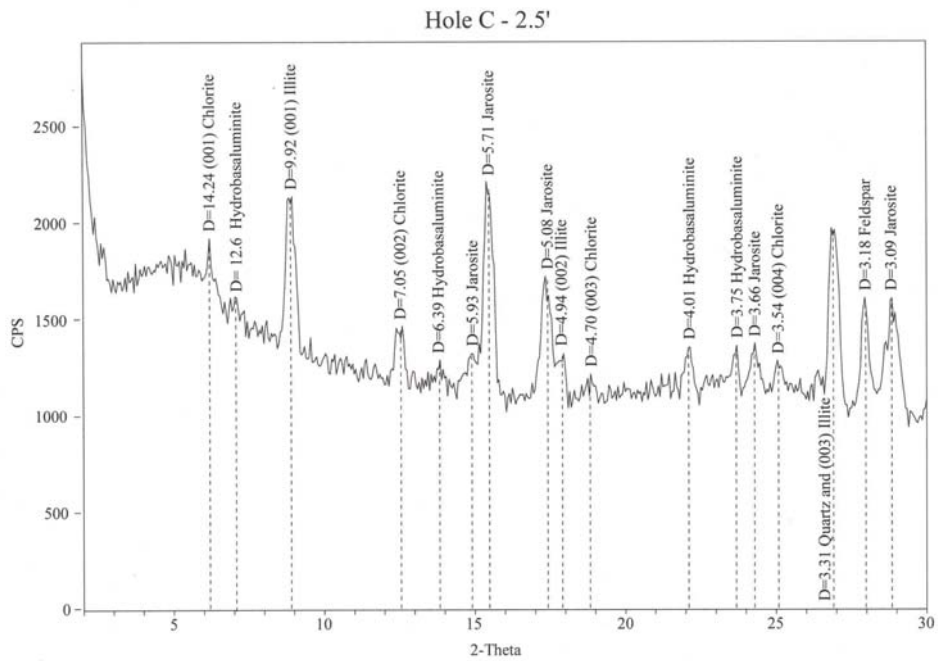


Figure 4.19: Diffractogram for Hole C – 2.5'.

At 3 feet, in Hole C, the diffractogram shows much more pronounced crystalline mica peaks as well as some chlorite minerals (Figure 4.20). There are large jarosite peaks in this sample as well. Again, there are three distinctive peaks of hydrobasaluminite at $d = 6.4, 4.02$ and 3.75 . The diffractogram of Hole C at 4 feet again shows chlorite and illite present as well as jarosite and feldspar (Figure 4.21). Peaks at 4.0 and 3.75 have not been identified. The five-foot sample at Hole C shows chlorite and illite as well as jarosite (Figure 4.22). The mystery peaks found in the previous three samples are not found in this sample.

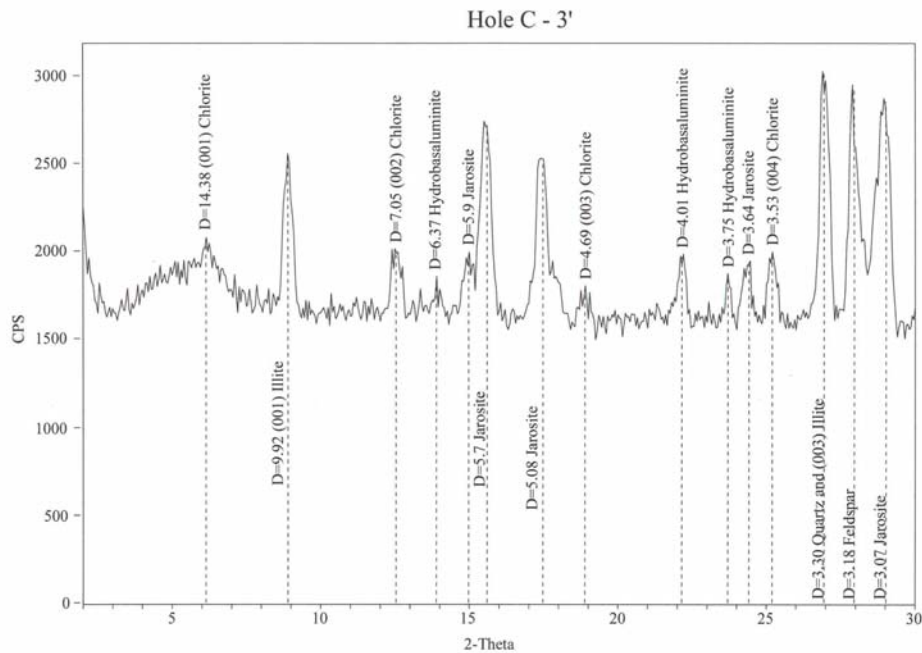


Figure 4.20: Diffractogram for Hole C – 3’.

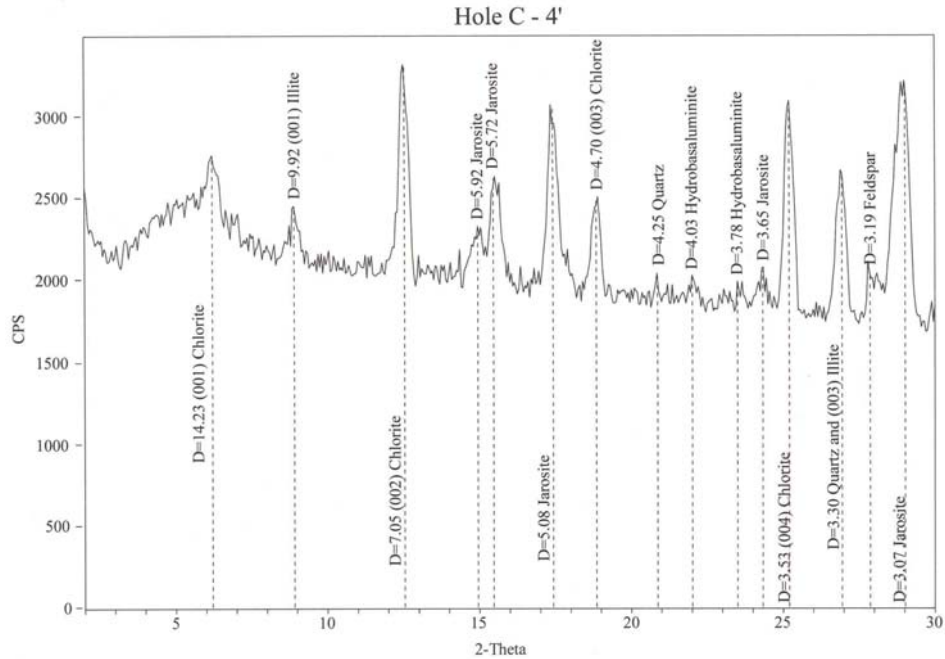


Figure 4.21: Diffractogram for Hole C - 4'.

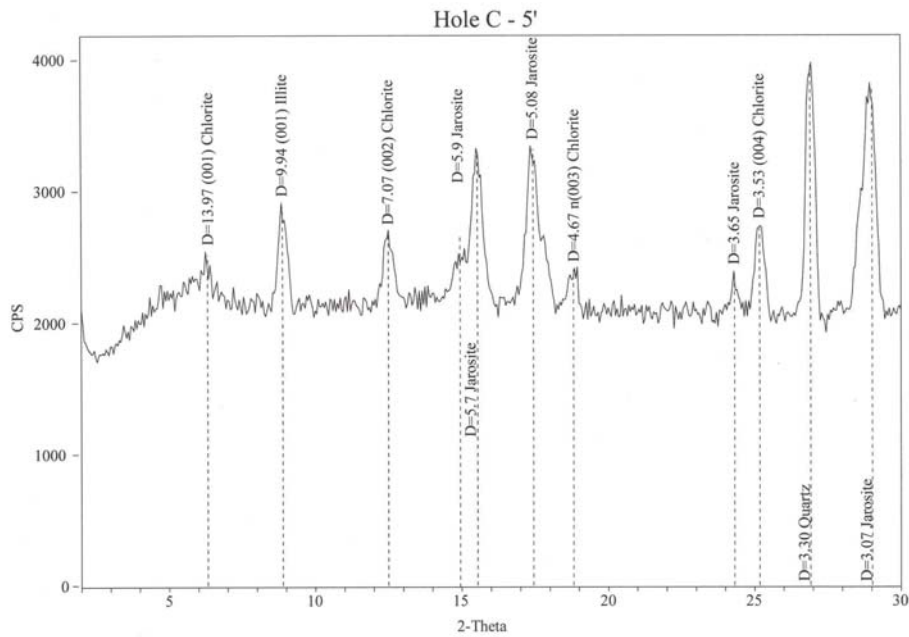


Figure 4.22: Diffractogram for Hole C - 5'.

Figure 4.23 presents the results of the XRD analysis of Hole D, 1 foot. This diffractogram shows the presence of chlorite and illite, along with some jarosite, quartz and some feldspar. The peaks are not very pronounced indicating some weathering of the

crystalline clay minerals took place. In the two-foot sample in the same hole, the diffractogram shows more crystallized clay minerals in the chlorite and illite peaks. There is no jarosite present in this sample. There is quartz and feldspar present at two feet (Figure 4.24).

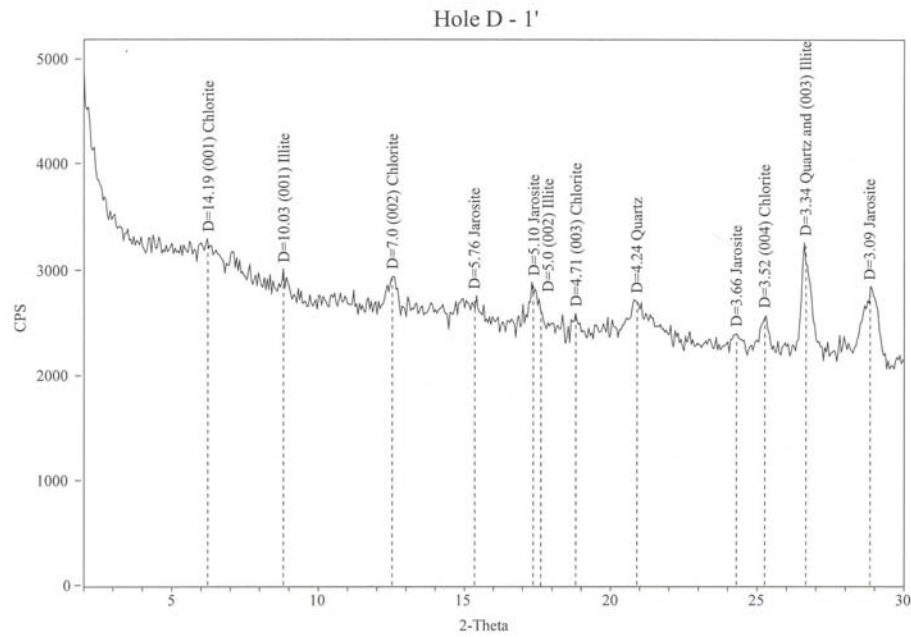


Figure 4.23: Diffractogram for Hole D – 1’.

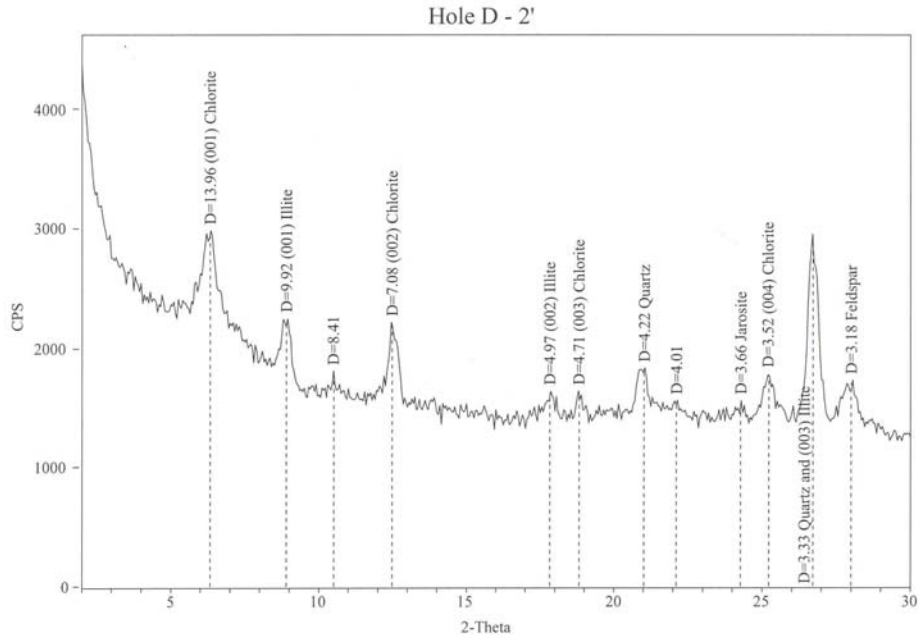


Figure 4.24: Diffractogram for Hole D – 2’.

Figure 4.25 presents the results of Well 9 at 1 foot. This diffractogram shows strong jarosite peaks, but not much clay. The clay mineral that stands out in this sample is chlorite, but the peaks are not very intense.

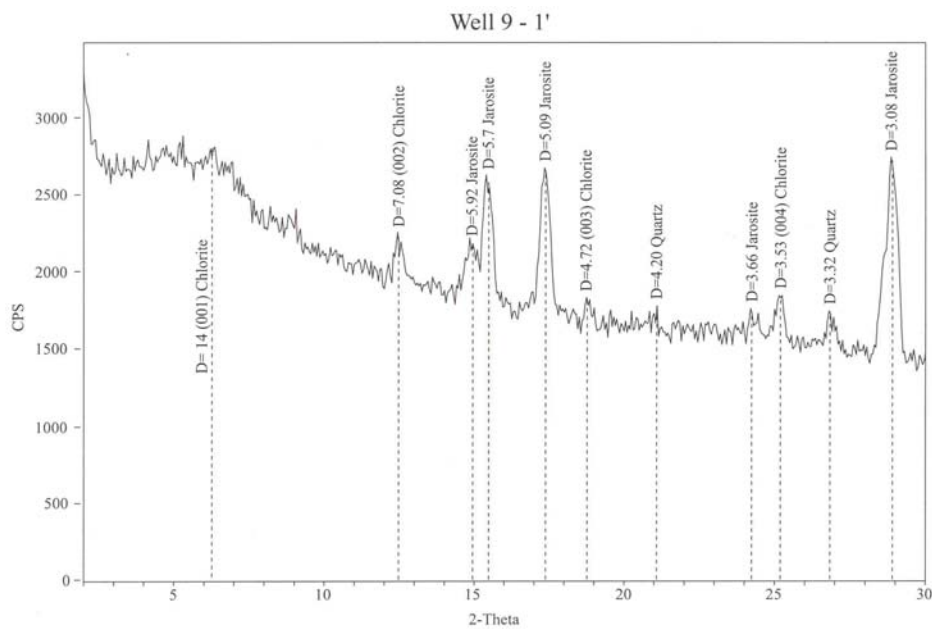


Figure 4.25: Diffractogram for Well 9 – 1’.

The sample at two feet show strong jarosite peaks and a possible illite clay mineral with (001) and a (003) peak readily visible (Figure 4.26). At 3 feet, the clay mineral chlorite is more apparent with some illite mixed in (Figure 4.27). Jarosite is present in this sample, but it is not as abundant.

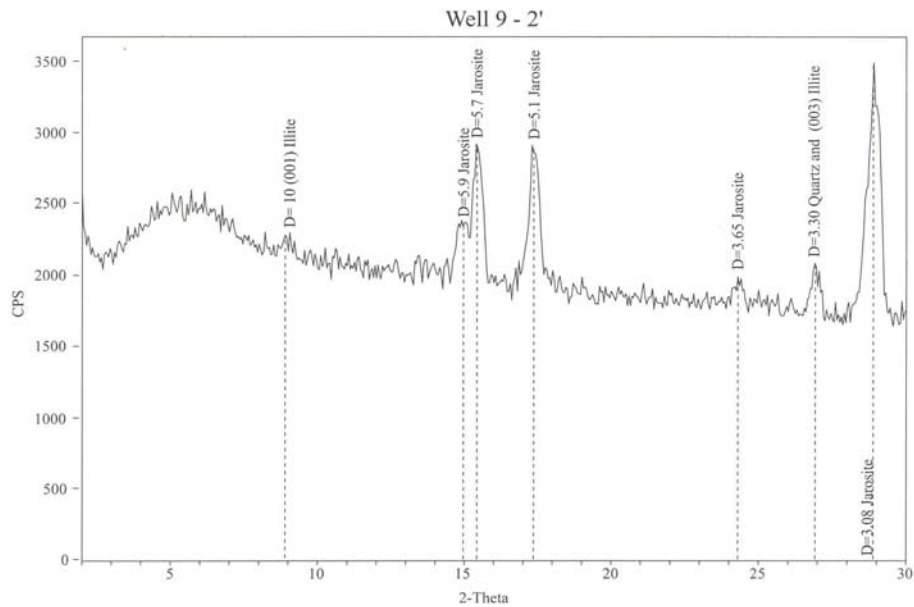


Figure 4.26: Diffractogram for Well 9 – 2’.

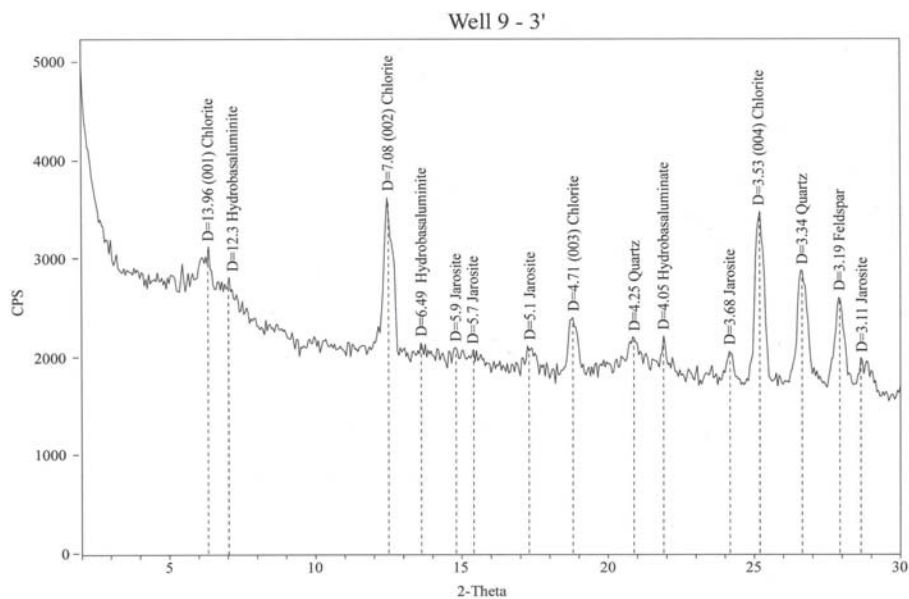


Figure 4.27: Diffractogram for Well 9 – 3’.

There are three distinctive peaks of hydrobasaluminite at $d = 6.37, 4.01$ and 3.75 . At 4 feet, the sample is much more crystalline and the chlorite and illite peaks are more apparent (Figure 4.28). There is also some smectite in this sample as well as quartz, feldspar and possible jarosite. The appearance of this smectite indicator was tested using the glycolated treatment as will be discussed in the following section.

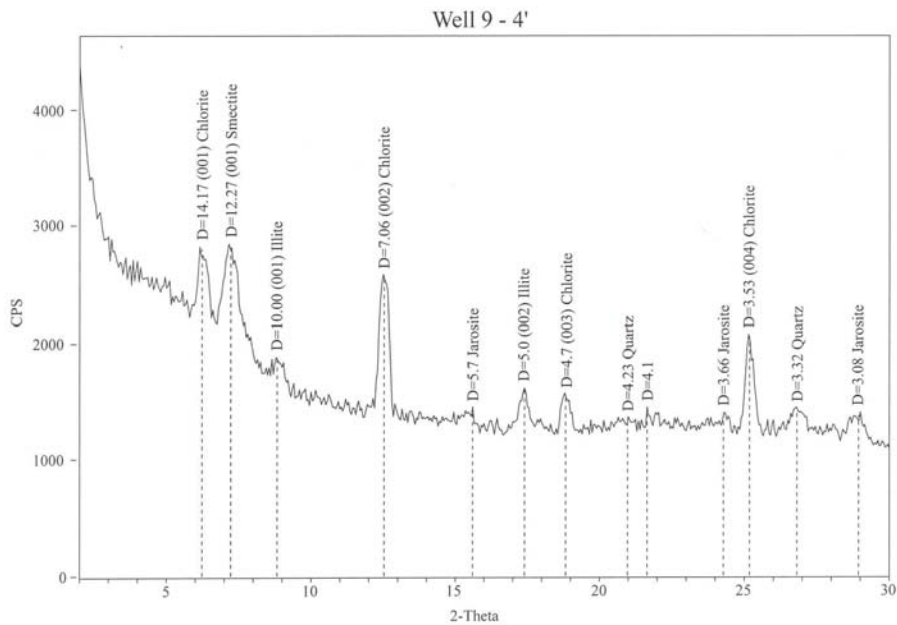


Figure 4.28: Diffractogram for Well 9 – 4’.

Figure 4.29 presents the results of Well5, spoon 2. This sample was taken from a split spoon during drilling and was mainly gravel and sand. This well was located in the stream channel, where river sediments overlie shallow bedrock. This sample is mainly comprised of jarosite and hydrobasaluminite and shows some poorly crystallized clay minerals.

Figure 4.30 presents the results of XRD testing on Well 2, Spoon 2 sample. This sample was also taken from a split spoon during drilling. This sample was also along the

stream channel, downstream of Well 5. The diffractograms of these two samples are similar. This sample shows chlorite and illite, however, little jarosite and hydrobasaluminite peaks are seen. There are peaks of hydrobasaluminite at $d = 12.2, 8.4, 6.3$ and 4.2 . Feldspar is present at a d spacing of 3.19 .

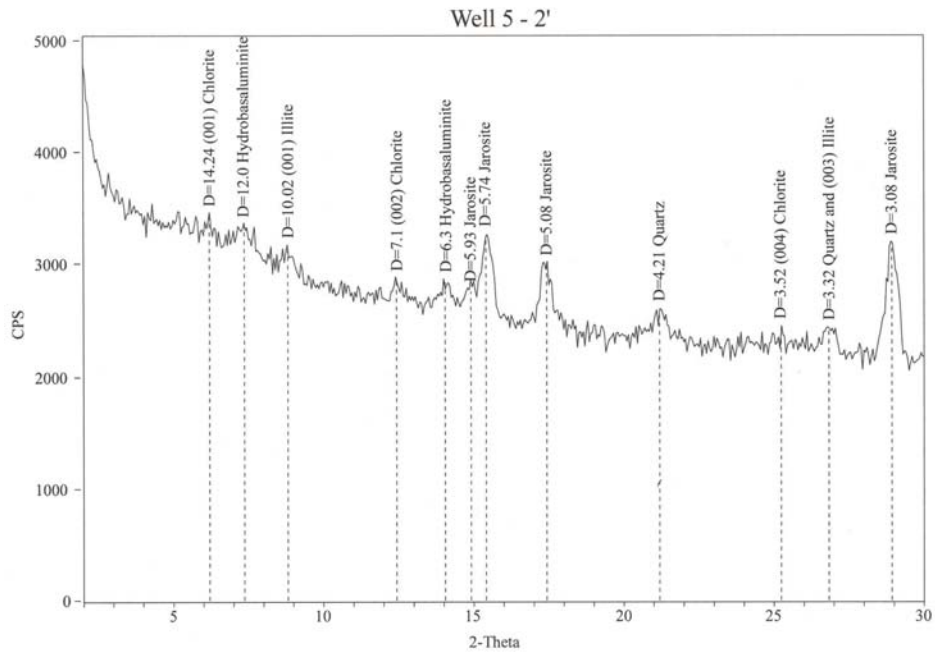


Figure 4.29: Diffractogram for Well 5 – 2’.

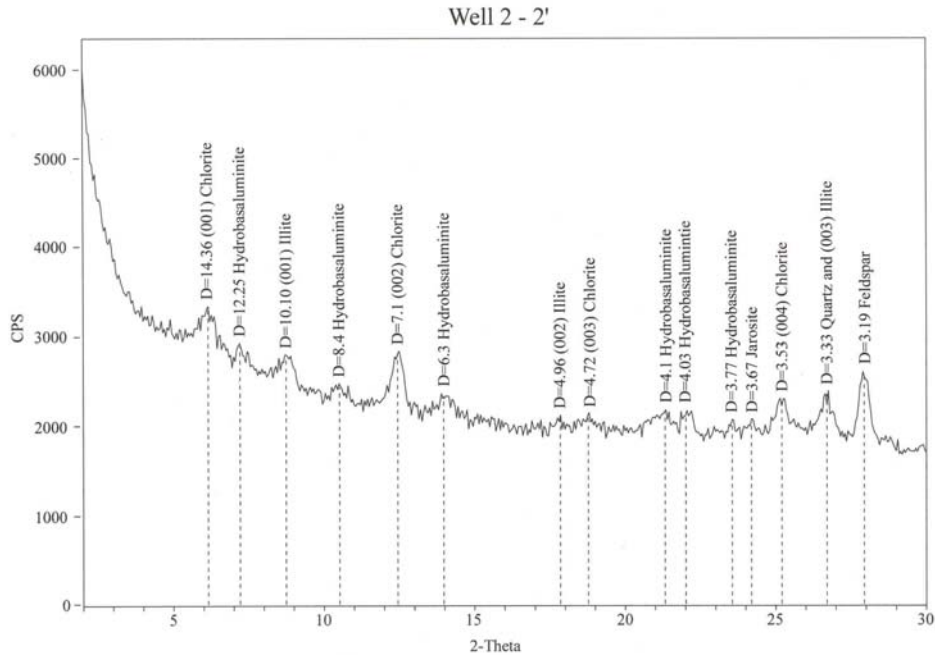


Figure 4.30: Diffractogram for Well 2 - 2'.

4.2.1 Glycolated Oriented Glass Slide

Six samples were chosen to perform additional slide treatments. The samples were chosen because they each had the characteristic smectite d-spacing peak at approximately 12. This theory was tested using the ethylene glycolation treatment on these six slides. Diffractograms were generated for the six samples and plotted on the same diffractogram of the previously run air-dried oriented slide results. An expansion of this peak to the left, indicates a swelling clay, or a smectite. Full size diffractograms are presented in Appendix C.

The soil sample from Well 6 at one foot showed a poorly defined peak at approximately 12.5 and another at 6.25. After glycolation, the peak at 12.5 did not shift to the left and was therefore thought to be an indicator of the aluminum iron hydroxide sulfate hydrobasaluminite (Figure 4.31).

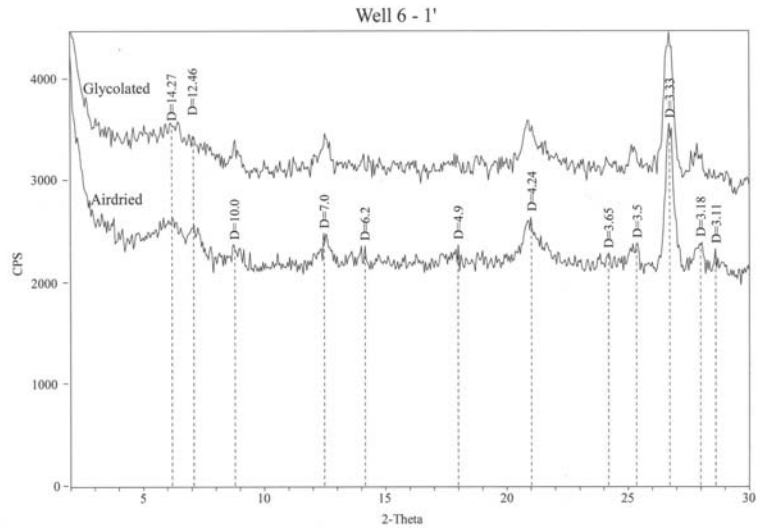


Figure 4.31: Determination of Swelling Clays in Well 6 – 1’ by the Ethylene Glycol Method.

The sample at Well 7, five feet, also had a peak at around 12.2, however, after glycolation, this peak again, did not appear to shift to the left, (Figure 4.32). It is believed that this peak indicates the presences of aluminum iron hydroxide sulfate, hydrobasaluminite.

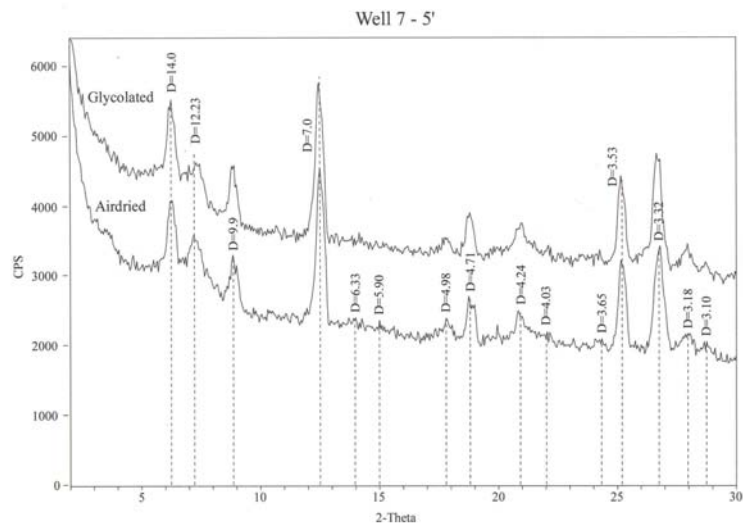


Figure 4.32: Determination of Swelling Clays in Well 7 – 5’ by the Ethylene Glycol Method.

Sample Well 9, 3 feet did not show a shift of the 12.3 peak and is again thought to be an aluminum iron hydroxide sulfate, hydrobasaluminite (Figure 4.33). Sample Well 9, 4 feet, shows a classic smectite shift after glycolation from 12.2 to 16.7, leaving the chlorite peak alone (Figure 4.34). This kind of shift is indicative of a pure smectite. The (002) peak of smectite can also be seen on the diffractogram.

Well 5 had a very weak 12.0 peak in the airdried diffractogram and after glycolation, did not seem to shift to the left. This sample is mainly poorly crystallized with the majority of the signal showing a large component of jarosite and the aluminum iron hydroxide sulfate, hydrobasaluminite (Figure 4.35). The 12.2 peak in the Well 2 diffractogram does not show a shift, therefore possibly indicating that the peak signals an aluminum iron hydroxide sulfate, hydrobasaluminite (Figure 4.36).

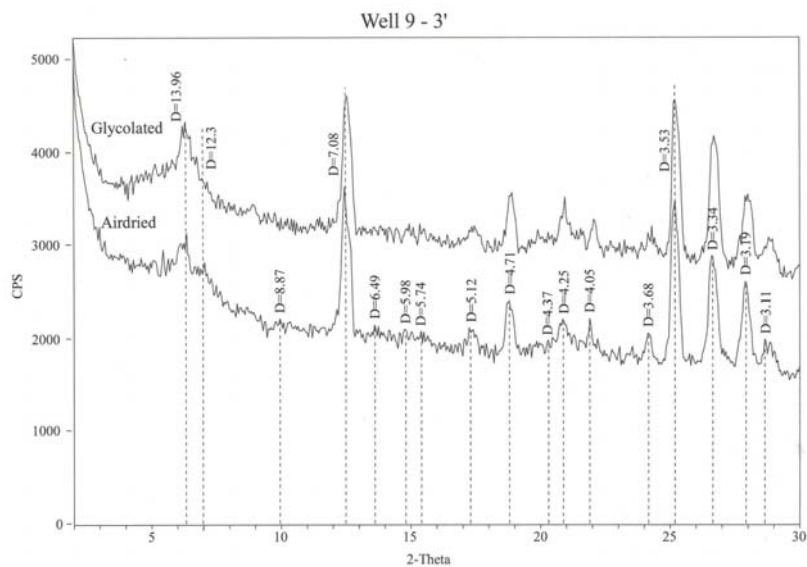


Figure 4.33: Determination of Swelling Clays in Well 9 – 3’ by the Ethylene Glycol Method.

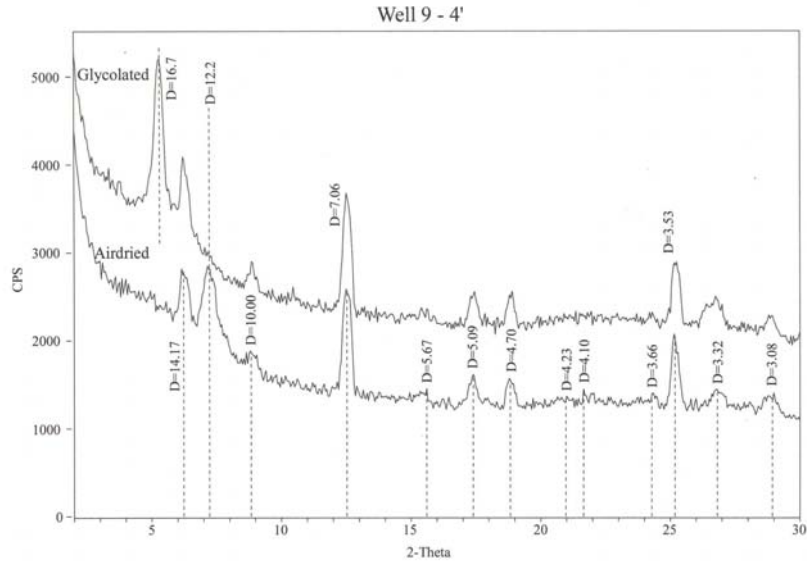


Figure 4.34: Determination of Swelling Clays in Well 9 – 4’ by the Ethylene Glycol Method.

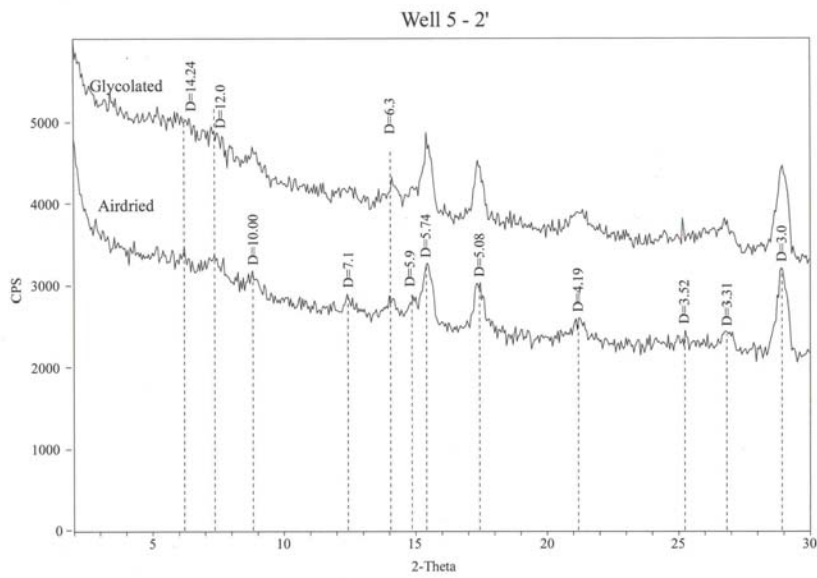


Figure 4.35: Determination of Swelling Clays in Well 5 – 2’ by the Ethylene Glycol Method.

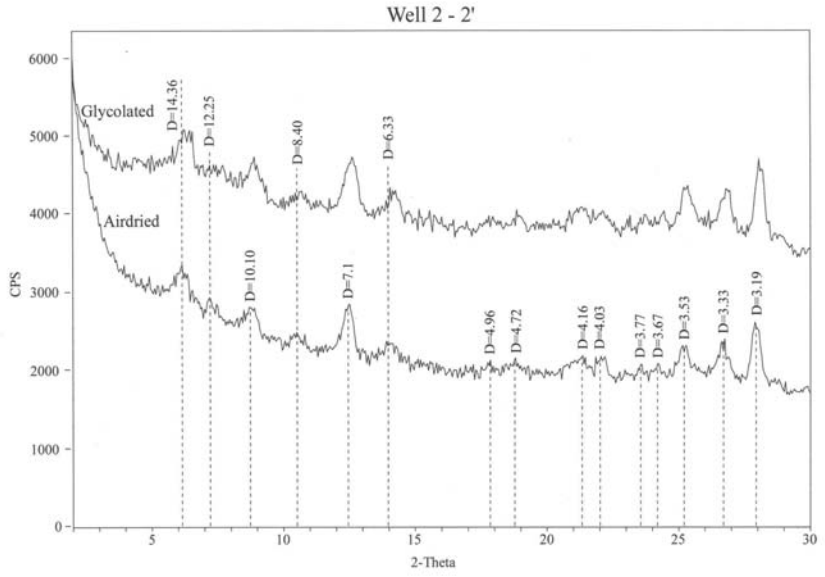


Figure 4.36: Determination of Swelling Clays in Well 2 – 2’ by the Ethylene Glycol Method.

5.0 DISCUSSION

5.1 Hydraulic Conductivity

The hydraulic conductivity of the site was determined using grain-size distribution predictive methods. The d_{10} and d_{50} (grain size relating to 10 % passing and 50 % passing respectively) of the samples taken from the site were used in theoretical equations relating the grain-size of the soil to hydraulic conductivity. The average hydraulic conductivity of the site using the three predictive methods ranged from 1.5 to 3×10^{-4} m/s (42 to 83 ft/day). These values are approximately one order of magnitude faster than results found by Gal (2000) from samples taken in the tailings pile, which ranged from 2.5 to 5×10^{-5} m/s (7.1 to 14 ft/day) (Table 5.1).

Table 5.1: Comparison of Average Hydraulic Conductivity Predictive Method Results.

	This Study k (m/s)	Previous Study k (m/s)
Hazen	2.95E-04	3.56E-05
Shepard	1.47E-04	2.46E-04
Beyer	2.17E-04	5.10E-05

This order of magnitude difference may be because the waste rock (tailings) consists of processed rock. This processed rock is made by grinding the ore to sand and silt sizes such that the finer particle sizes dominate the tailings environment. The finer particles would fill more void spaces, not allowing water to flow as freely through the matrix, whereas the natural soil generally consists of larger particles, and a higher porosity, and therefore, a slightly faster hydraulic conductivity.

These hydraulic conductivities are simply averages however and it must be noted that hydraulic conductivity and groundwater flow is site specific (Robertson, 1994). Groundwater flow conditions in mine tailings and in the natural site vary widely from location to location. Using just the Shepard method, the hydraulic conductivities across the site range from 2.25×10^{-5} m/s (6 ft/day) in Well 7 to 3.0×10^{-4} m/s (85 ft/day) in Hole A. Although these predictive methods provide a good estimation of the hydraulic conductivities throughout the site, and correlate within one order of magnitude with previous bail tests performed, results should be used with caution, as the variability in mineralogy and therefore, hydraulic conductivity, has been shown to be significant.

5.2 Mineralogy

Figure 5.1 presents the results of Well 7 compiled by depth.

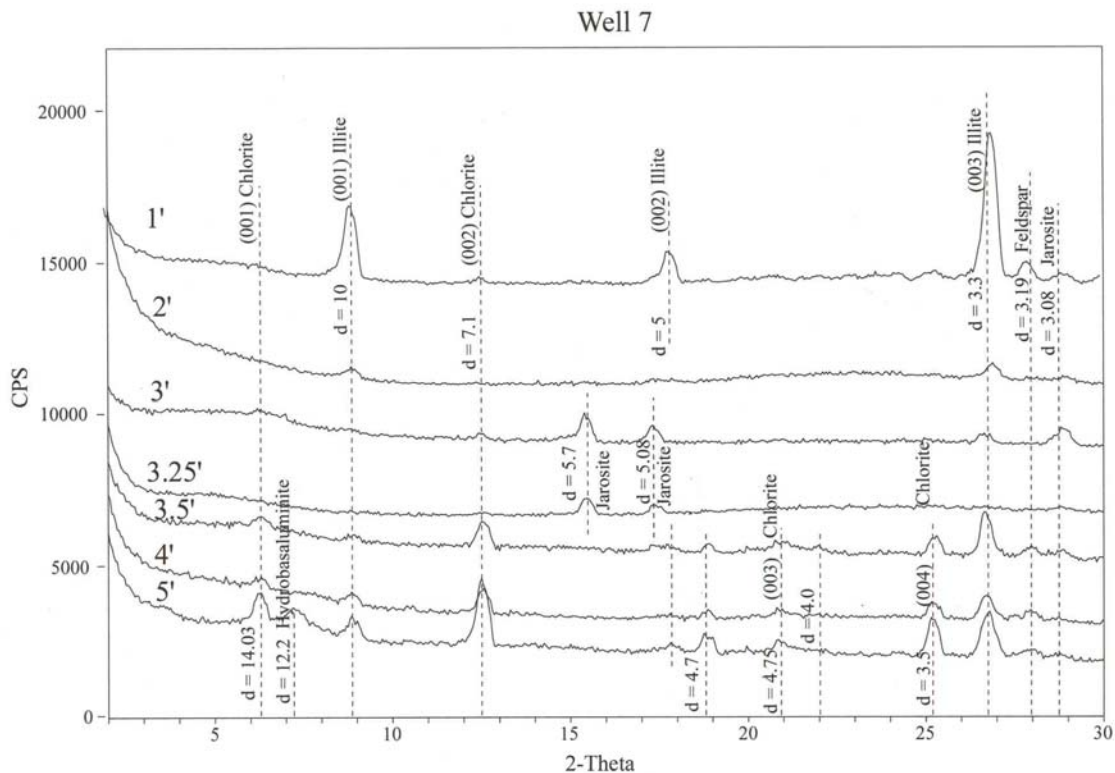


Figure 5.1: Diffraction Results Compiled by Depth in Well 7.

This profile is interesting because it shows that in the top two feet, the soil is mainly illitic. At three feet, there is no longer any noticeable crystalline clay, and the Potassium Iron Sulfate Hydroxide, jarosite, component is readily visible for at least half a foot. This may indicate the hardpan layer marking the zone of higher pH in the profile. Below this layer, strong chlorite peaks are seen in the deeper samples to five feet where bedrock was found. These three deepest samples show both illite and chlorite mineralogy and the deepest sample at five feet also shows an aluminum iron hydroxide sulfate, hydrobasaluminite peak as shown in Figure 4.32. The three deepest samples also have an abundance of quartz content that show in the diffractograms. This profile is a clue about weathering patterns in the soil matrix at this particular location. There is a distinctive layer of jarosite between approximately 2 and 3.5 feet below the surface, which means that this is an area of Fe^{+3} hydrolysis, which has not had a chance to change into an oxyhydroxide (goethite), and it is also a layer of low pH. The presence of hydrobasaluminite in the 4 and 5-foot layers suggests that the water table rarely retreats below this depth and that the pH of this soil is between approximately 4.5 and 5. If the water table did retreat past these layers, the hydrobasaluminite would dehydrate irreversible to basaluminite and would show different diffractogram patterns. The mineralogy in this profile suggests an increase in pH with depth at this particular location at Davis Mine.

Figure 5.2 presents the results of Hole C compiled by depth. Hole C was augured in the second tailings pile between Wells 3 and 4. In this profile, the first two feet consist of only jarosite. Then, as the hole gets deeper, strong illitic crystalline minerals are found with some weak chlorite peaks. By the time four feet is reached, the chlorite signals get

much stronger. The jarosite content continues throughout the profile. There is a distinctive layering of hydrobasaluminite between depths 2.5 and 4 feet. This profile is similar to Gal's (2000) findings from the tailings pile near Mine Shaft #1, however, Hole C, from this study, shows a much more pronounced surface layer of jarosite devoid of any clay minerals. Hole C has a similar profile to that of Well 9 where the jarosite layer is located in the first two feet without any other clay minerals present. However, Hole C's profile is quite different than the Well 7 profile, where jarosite only occurs in a half-foot band and is absent at every other depth. In Hole C, the exclusively jarosite layer is located at the first two feet, whereas in Well 7, it was located between 3 and 3.5 feet below the surface. In Hole C, there is layering of the aluminum iron hydroxide sulfate, hydrobasaluminite, occurring in the 2.5 and 3 and 4 foot samples with peaks at $d = 6.37$, 4.01 and 3.75 Å.

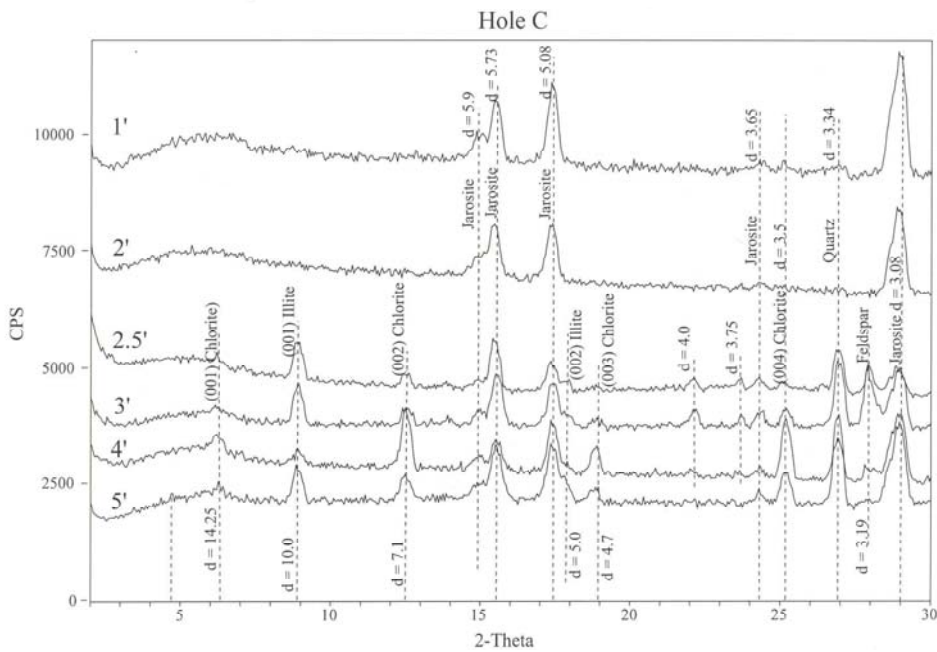


Figure 5.2: Diffractogram Results Compiled by Depth in Hole C.

Figure 5.3 presents the results of Hole D compiled by depth. There are two depths recorded at this location. These two depths show that the clay minerals in the first foot of this profile are not well crystallized, although it is possible to tell that there is chlorite and illite present as well as some jarosite. In the second foot of the profile the clay minerals are much more crystalline and show more intense peaks. This sample does not contain any jarosite.

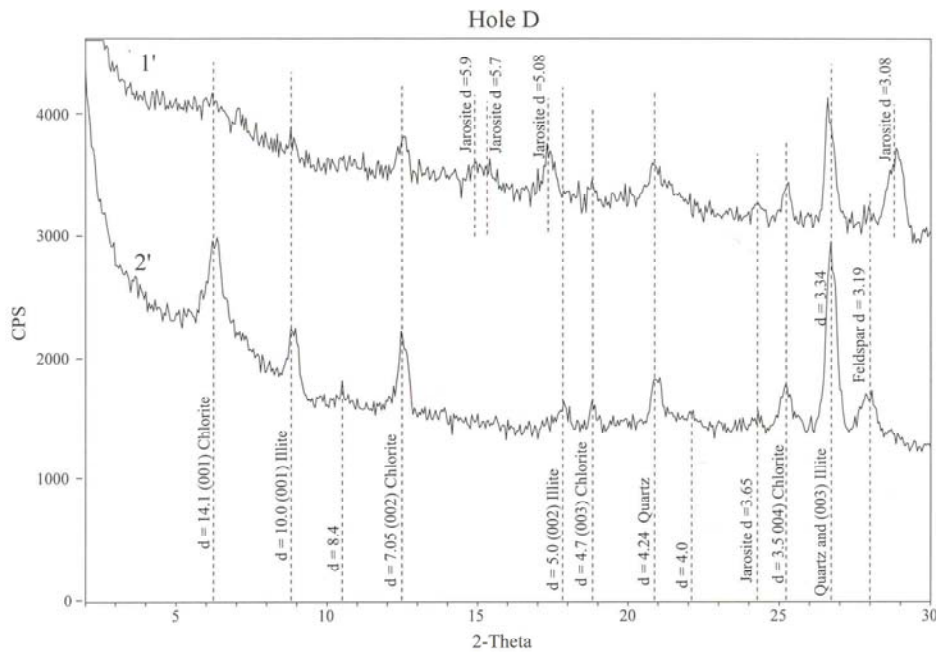


Figure 5.3: Diffractogram Results Compiled by Depth in Hole D.

Figure 5.4 presents the results of Hole A compiled by depth. Both one and two foot samples show strong Chlorite and Illite peaks along with Jarosite. The one-foot sample contains some aluminum iron hydroxide sulfate, hydrobasaluminite, as seen by a

d spacing of around 11. This sample also includes some feldspar. Bedrock was hit at 2.5 feet at this location.

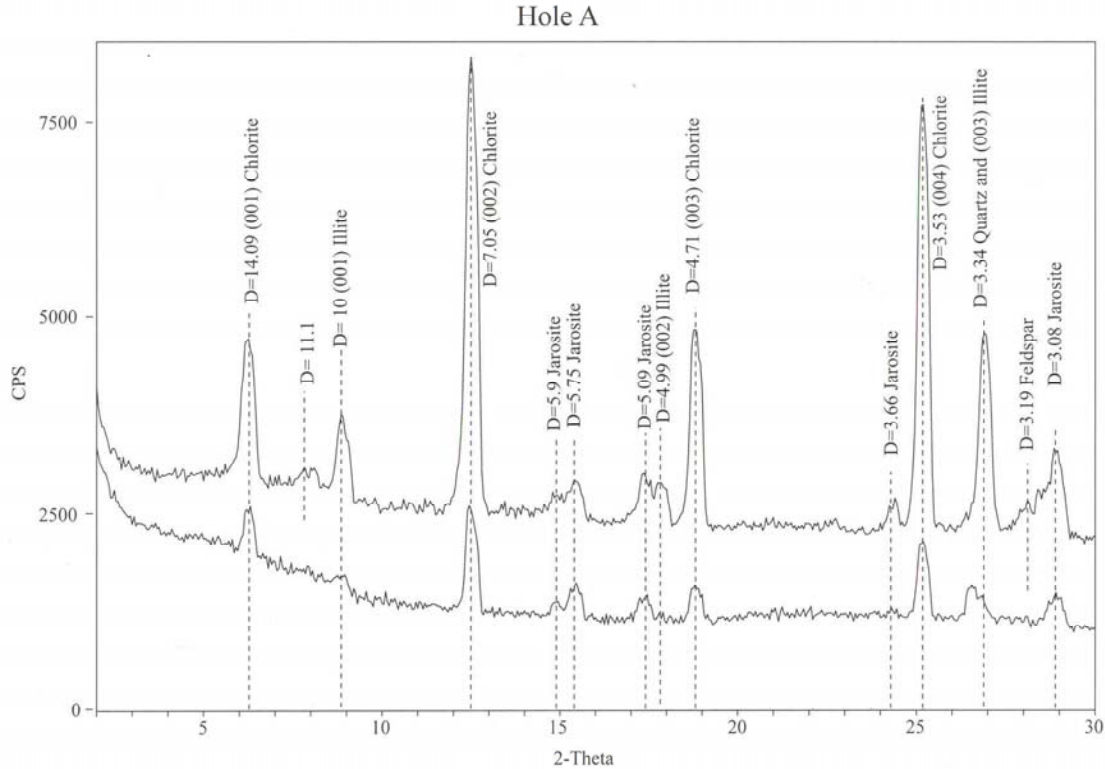


Figure 5.4: Diffractogram Results Compiled by Depth in Hole A.

Figure 5.5 presents the results of Well 9 compiled in profile. In the first two feet of this core, the dominant component is jarosite with some weak chlorite and illite peaks. By depths 3 and 4 feet, the jarosite indicators have diminished and the chlorite and illite peaks have become much more pronounced. At 4 feet, there is also a strong smectite peak, as was proved using a glycolation technique. It is rather curious as to why there is smectite at Davis Mine and, as of this date, no suitable explanation is available. There is still some jarosite in these two deeper samples, however, as can be seen, the peaks are all but gone.

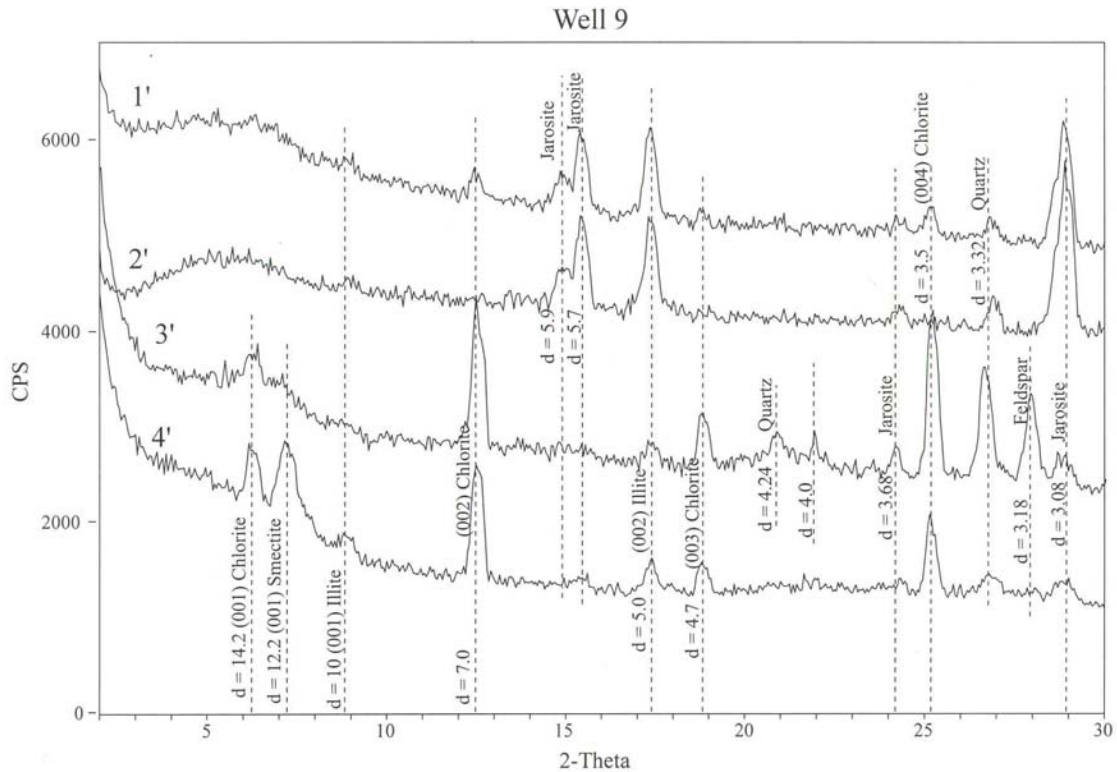


Figure 5.5: Diffractogram Results Compiled by Depth in Well 9.

6.0 SUMMARY AND CONCLUSIONS

This report presents the results of soil classification and X-Ray Diffraction tests of thirty soil samples collected from Davis Mine in Rowe, Massachusetts. These tests were conducted at the GeoChemistry Laboratories, University of Massachusetts Amherst between 21 May and 10 August 2003. These tests were conducted in general accordance with ASTM D422-63 Standard Test Method for *Particle-Size Analysis of Soils* (ASTM 1998) the “Semi-Quantitative” XRD Method discussed by Moore and Reynolds (1996).

The following are the average hydraulic conductivity results and mineralogical content at each sample location.

- Well 6 – 5.1×10^{-5} m/s: Chlorite, Illite, Hydrobasaluminite, Quartz, Feldspar and Apatite

- Well 7 – 1.5×10^{-4} m/s: Chlorite, Illite, Layered Hydrobasaluminite, Layered Jarosite, Quartz and Feldspar
- Sample 02-01 – 5.0×10^{-5} m/s: Chlorite, Illite, Jarosite, Quartz and Feldspar
- Sample 02-03 – 2.5×10^{-4} m/s: Illite and Jarosite
- Sample 02-07 – 6.5×10^{-5} m/s: Chlorite, Illite, Hydrobasaluminite, Jarosite, Quartz and Feldspar
- Sample 02-09 – NA: Jarosite, Hydrobasaluminite, Quartz and Feldspar
- Sample 02-10 – 1.5×10^{-4} m/s: Chlorite, Illite, Jarosite, Quartz and Feldspar
- Hole A – 5.0×10^{-4} m/s: Chlorite, Illite, Jarosite, Quartz and Feldspar
- Hole B – 1.6×10^{-4} m/s: Jarosite
- Hole C – 2.8×10^{-4} m/s: Chlorite, Illite, Layered Jarosite, Layered Hydrobasaluminite, Quartz and Feldspar
- Hole D – 6.5×10^{-5} m/s: Chlorite, Illite, Layered Jarosite, Quartz and Feldspar
- Well 9 – 1.8×10^{-4} m/s: Chlorite, Smectite, Illite, Layered Jarosite, Layered Hydrobasaluminite, Quartz and Feldspar
- Well 5 – 7.0×10^{-5} m/s: Chlorite, Illite, Jarosite, Hydrobasaluminite and Quartz
- Well 2 – 9.0×10^{-5} m/s: Chlorite, Illite, Hydrobasaluminite, Quartz and Feldspar

The soil conditions were not uniform throughout the site, with hydraulic conductivities ranging approximately one order of magnitude across the site from 5.0×10^{-4} m/s to 5.0×10^{-5} m/s. The clay mineralogy was generally similar across the site with a large amount of chlorite and illite, with layered areas of jarosite and hydrobasaluminite occurring at varying depths. Overall, the subsurface exploration and laboratory tests produced results that were consistent with the general geology of the area.

7.0 REFERENCES

Alyamani, M. and Sen, Z. 1993. Determination of Hydraulic Conductivity from Complete Grain-Size Distribution Curves. *Groundwater*, V. 31, No. 4, pp. 551-555.

Bannister, F.A. and Hollingworth, S.E. 1948. *Nature*. v. 162, pp.565.

Blowes, D.W., Reardon, E.J., Jumbor, J.L. and Cherry, J.A. 1991. The formation and Potential Importance of cemented layers in inactive Sulfide Mine Tailings. *Geochimica et Cosmochimica Acta*, Vol. 55, pp. 965-978.

Bouwer, H. and Rice, R.C. 1976. A slug test for determining hydraulic conductivity of unconfined aquifers with completely or partially penetrating wells. *Water Resources Research*, Vol. 12, pp. 423-428.

Brown, X. 1960. History of Rowe, Massachusetts: 1882-1911. The Rowe Historical Society Publication. 3rd Edition. White Eagle Printing, Adams, MA.

Callen, R.A. 1984. Clays of the Palygorskite-Sepiolite Group: Depositional Environment, Age and Distribution. Singer, A. and Galan, E. (eds). *Developments in Sedimentology. Palygorskite-Sepiolite. Occurrences, Genesis and Uses.*

Chamley, H. 1989. *Clay Sedimentology.* Springer-Verlag, Berlin. 623 p.

Cravotta, C.A. 1994. Secondary Iron-Sulfate Minerals as Sources of Sulfate and Acidity. Chapter 23: Environmental Geochemistry of Sulfide Oxidation. Ed. Alpers, C.N. and Blowes, D.W. pp. 345-364.

Darcy, H. 1856. *Les fontaines publiques de la ville de Dijon.* Paris: Victor Dalmont.

Field, S.W. 1985. Mineralogy and Petrology of the Davis Mine, Rowe, Massachusetts. M.S. Thesis, Department of Geology and Geography, University of Massachusetts, Amherst.

Forstner, U; Salomons, W., eds. *Environmental Management of Solid Waste.* Springer-Verlag Berlin Heidelberg. 1988.

Freeze, R.A. and Cherry, J.A. 1979. Groundwater. Prentice Hall. Englewood Cliffs, NJ.

Gál, N.E. 2000. The impact of acid-mine drainage on groundwater quality, Davis Pyrite Mine, Massachusetts. Ph.D. Dissertation, Department of Geology and Geography, University of Massachusetts, Amherst.

Germain, M.D., Tasse, N. and Bergeron, M. 1994. Limit to Self-Neutralization in Acid Mine Tailings. Chapter 24: Environmental Geochemistry of Sulfide Oxidation. Ed. Alpers, C.N. and Blowes, D.W. pp. 365-379.

Hayden, P.L. and Rubin, A.J. 1974. Aqueous-Environmental Chemistry of Metals, pp. 317-81.

Hazen, A. 1893. Some Physical Properties of Sands and Gravels. Massachusetts State Board of Health, 24th Annual Report.

Hazen, A. 1911. Discussion: Dams on Sand Foundations. *Transactions, American Society of Civil Engineers*, Vol. 73, pp. 199.

Hvorslev, M.J. 1951. Time Lag and Soil Permeability in Ground Water Observations. U.S. Army Corps of Engineers Waterway Experimentation Station, Bulletin 36.

Krumbein, W.C. and Monk, G.D. 1942. Permeability as a Function of the Size Parameters of Unconsolidated Sand. American Institute of Metallurgical Engineers, Technical Publication.

Masch F.E. and Denny, K.J. 1966. Grain-Size Distribution and its effect on the permeability of unconsolidated sands. Water Resources Research. Vol. 2, pp. 665-677.

Moore, D.M. and Reynolds, R.C. 1996. X-Ray Diffraction and the Identification and Analysis of Clay Minerals (2nd Edition). Oxford University Press, NY.

Norris, S.E. and Fiddler, R.E. 1965. Relation of Permeability to Grain Size in a Glacial-Outwash Aquifer at Piketown, Ohio. U.S. geological Survey Professional Paper 525-D, pp. 203-206.

Shepherd, R.G. 1989. Correlations of Permeability and Grain Size. Groundwater, Vol. 27, No. 5, pp. 633-638.

Singer, P.C. and Stumm, W. 1970. Acidic Mine Drainage: The Rate Determining Step. Science, Vol. 167, pp. 1121-1123.

Uma, K.O., Egboka, B.C.E. and Onuoha, K.M. 1989. New Statistical Grain-Size Method for Evaluating the Hydraulic Conductivity of Sandy Aquifers. Journal of Hydrology, Vol. 108, pp. 343-366.

Vukovic, M. and Soro A. 1992. Determination of Hydraulic Conductivity of Porous Media from Grain-Size Composition. Water Resources Publication. pp. 16.